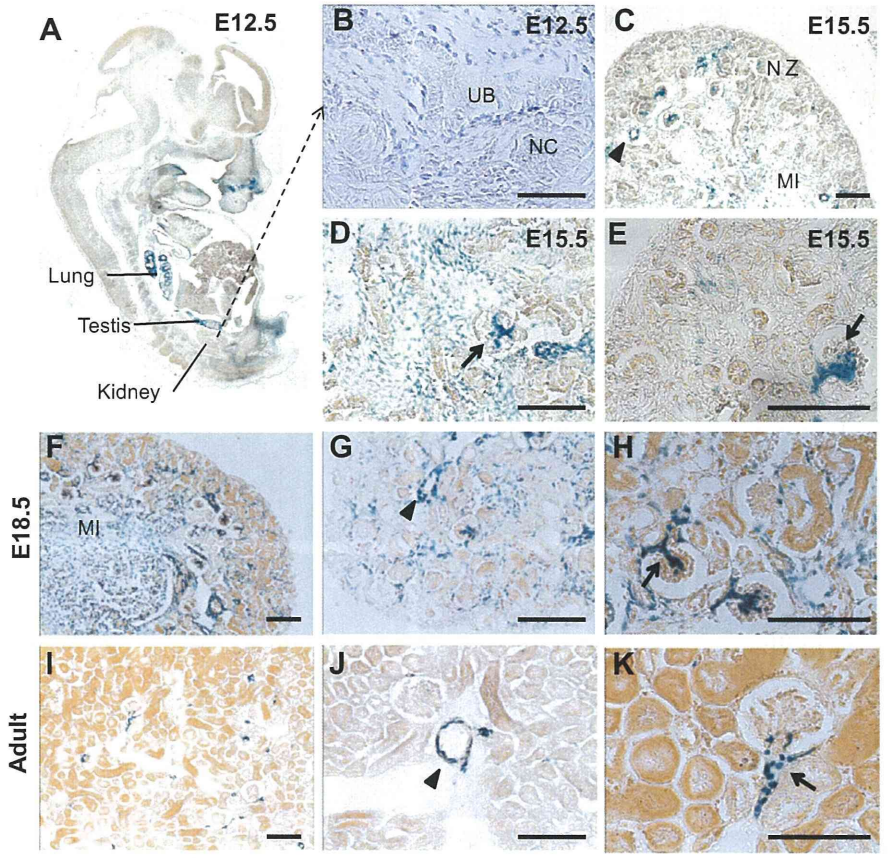

Fig. 2. β-Galactosidase staining in the *Ednra-lacZ* embryonic and adult kidneys. (A and B) A section of an E12.5 embryo stained for β-galactosidase activity. A is a low magnification image of the whole embryo and B is a high magnification image of the renal region of A. Renal *LacZ* signals can be detected but they are much weaker than those of the lung and testis. Signals are detected in mesenchyme around ureteric buds (UB), but not in nephrogenic condensates (NC). (C–E) Sections of the E15.5 kidneys stained for β-galactosidase activity. C is a low magnification image. (D and E) Higher magnification images of the medullary interstitial region and cortical nephrogenic region, respectively. (F–H) Low (F) and high (G and H) magnification images of E18.5 kidney sections stained for β-galactosidase activity. Basic expression pattern of *LacZ* in the E18.5 sections is the same with that of E15.5 ones. Abundant *LacZ* expression is detected throughout the medullary interstitium (C, D and F), but, compared with this, few signals can be detected in the nephrogenic mesenchyme of the cortical region (E). *LacZ* signal are detected around vessels (C, G, arrowheads) and the JG region including small vessels and intraglomerular mesangial cells (E, H, arrows). Renal tubules are apparently *LacZ*-negative. (I–K) Low (I) and high (J and K) magnification images of kidney sections of adult (2 months) mice stained for β-galactosidase activity. *LacZ*-expressing cells are detected around vessels (J, arrowhead) and in the JG region with adjacent small vessels (K, arrow), but are not detected in renal tubules as in embryonic sections. Compared to the developing kidney, *lacZ*-expressing cells were much decreased in the interstitium and inside the glomerulus (I). All the sections are counterstained with orange G. MI, medullary interstitium, NZ, nephrogenic zone. Scale bars: 100 μm.

expression in developing interstitial mesenchyme may be confined to pericytes.

1.3. Inclusion of renin-producing cells in Ednra–EGFP-positive cell population

Next we performed double immunostaining for EGFP and renin on *Ednra*$^{EGFP/+}$ kidney sections to confirm that renin-producing cells are Ednra-positive. At E18.5, renin-expressing cells were found not only in the JG region (Fig. 4A–A″) but also in vessels outside the JG region (Fig. 4B–B″) as previously described (Sauter et al., 2008). These renin-producing cells were always found to express EGFP (Fig. 4A–A″ and B–B″). In the adult kidneys, renin expression became restricted to cells within the JG region, which were also included within EGFP-positive cell population encompassing the afferent and efferent arterioles (Fig. 4C–C″).

2. Discussion

In the present study, *Ednra*-positive cells in the kidney were clearly distinguished by marker gene expression. Renal *Ednra* expression was first observed in mesenchymal cells around the ureteric bud around E12.5. Thereafter, *Ednra* expression was broadly distributed in vascular smooth muscle cells, JG cells and mesenchymal cells in the interstitium until neonatal stages. After growth, the expression became confined to vascular smooth muscle cells, pericytes and renin-producing JG cells. By contrast, most cells in the nephron and vascular endothelial cells did not express *Ednra*. This pattern is quite distinct from that of *Ednrb*, which is abundantly expressed in tubular epithelial cells and vascular endothelial cells (Chow et al., 1995; Nangaku et al., 2002; Terada et al., 1992).

Kidney development initiates with the interaction between the Wolffian duct and metanephric mesenchyme (Vainio and Lin, 2002). The Wolffian duct generates the ureteric bud, which then invades the metanephric blastema to induce nephrogenic epithelial condensates destined to develop into nephrons. On the other hand, stromal cell progenitors that are not destined to nephrons are thought to become interstitial mesenchyme, vascular smooth muscle cells and JG cells (Humphreys et al., 2010; Kobayashi et al., 2008; Maric et al., 1997; Sequeira Lopez et al., 2004, 2001). Thus, *Ednra* expression may be linked with non-epithelial fate determination and differentiation of mesenchyme. This is in sharp

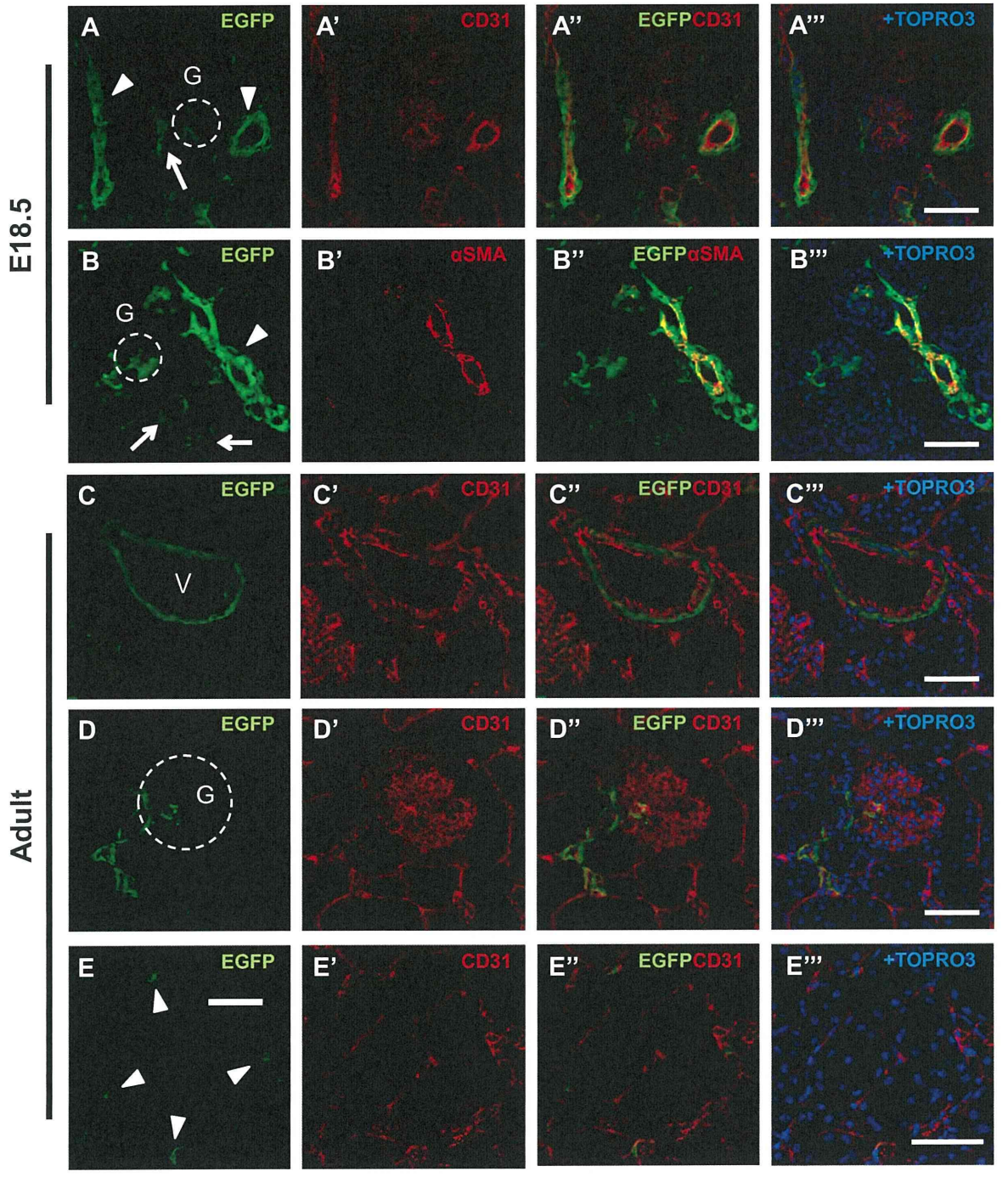

Fig. 3. Expression patterns of EGFP, CD31 and αSMA in *Ednra–EGFP* kidneys. Sections of E18.5 (A–A‴, B–B‴) and adult (C–C‴, D–D‴, E–E‴) kidneys immunostained for EGFP (A–E, A″–E″; green), CD31 (A′, A″, C′, C″, D′, D″, E′, E‴; red), αSMA (B′, B″; red), and merged with TO-PRO-3 staining for nuclei (A‴–E‴; blue). In E18.5 kidneys, EGFP-positive cells are detected around CD31-positive vascular endothelial cells (A–A‴, arrowheads), and in the JG region (A–A‴, arrow). EGFP was co-expressed with αSMA in vessels (B–B‴, arrowhead), but not in the JG region (B–B‴, around glomerulus). EGFP-positive but αSMA-negative cells in the interstitium are indicated with arrows (B–B‴). In the adult kidneys, EGFP-positive cells are detected around CD31-positive endothelial cells (C–C‴) and in the JG region (D–D‴). Compared to the embryonic kidneys, EGFP signals are much decreased inside the glomerulus (D–D‴). EGFP-positive cells in the interstitium are associated with CD31-positive endothelial cells (E and E‴). G: glomerulus. Scale bars: 50 μm.

contrast to the expression of Ednrb, which is abundantly expressed in tubular epithelial cells that are derived from nephrogenic mesenchyme.

In addition to vascular smooth muscle cells, renin-producing JG cells shows intense staining for Ednra expression. This result is consistent with previous finding that Edn directly inhibit cAMP-dependent renin production through Ednra in cultured JG cells (Ryan et al., 2002). JG cells were postulated to derive from smooth muscle cells in the past (Owen et al., 1995). However, Sequeira Lopez et al. have shown that renin-producing precursor cells differentiate into a diversity of cells including smooth muscle cells (Sequeira Lopez et al., 2004, 2001). Furthermore, Matsushita

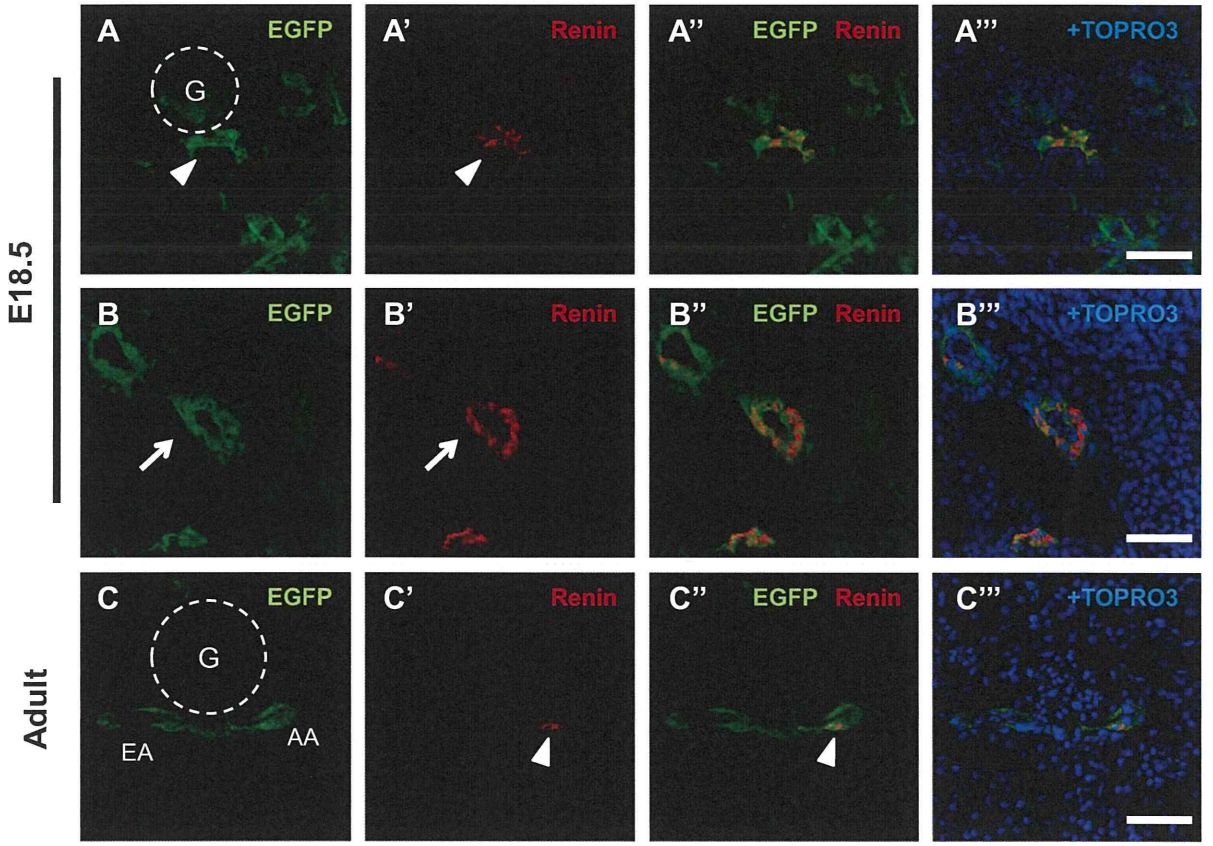

Fig. 4. Co-localization of EGFP and renin in *Ednra–EGFP* kidneys. Sections of kidneys of E18.5 (A–A‴, B–B‴), and adult (C–C‴) mice, immunostained for EGFP (A–C, A″–C‴; green), renin (A′–C′, A″–C″; red), and merged with TO-PRO-3 staining for nuclei (A‴–C‴; blue). In both the E18.5 (A–A‴) and adult (C–C‴) JG region, rennin-producing cells are EGFP-positive (arrowheads). In E18.5 kidneys, rennin-producing cells are also detected in vessels outside the JG region, which are also EGFP-positive (arrows) (B–B‴). G: glomerulus. Scale bars: 50 μm.

et al. have demonstrated the presence of mesenchymal stem cells that may give rise to smooth muscle cells through renin-producing precursors (Matsushita et al., 2010). Although the origin of JG cells and their relationship to smooth muscle cells in the lineage hierarchy is still controversial, *Ednra* expression may serve as a hallmark for non-epithelialized metanephric descendants.

In the present study, *Ednra* expression appears to decrease in mesangium and interstitium after growth. On the other hand, Ednra has been implicated in various diseases involving these cell populations, such as glomerulonephritis and renal intestinal fibrosis (Brochu et al., 1999; Sorokin and Kohan, 2003). In these pathological conditions, *Ednra* expression may be re-activated in proliferative mesangial and/or mesenchymal cells, where Ednra may mediate a mitotic signal to contribute to disease progression.

It has been known that the Edn system is deeply involved in various renal (patho)physiology. However, dissection of its diverse action is difficult possibly because their different effects on the nephron and vasculature can hardly be discriminated (Dhaun et al., 2006). *Ednra*-knock-in mice may serve as a useful tool in such studies by enabling us to identify and isolate *Ednra*-expressing cells in various conditions.

3. Materials and methods

3.1. Mice

Ednra$^{lacZ/+}$ (*lacZ*-knock-in) and *Ednra*$^{EGFP/+}$ (*EGFP*-knock-in) mice, described previously (Asai et al., 2010; Sato et al., 2008a), were maintained on an ICR-background. Mice were housed in an environmentally controlled room at 23 ± 2 °C, with a relative humidity of 50–60% and under a 12L–12D light cycle. Genotypes were determined by PCR on tail-tip or amnion DNA using specific primers. Embryonic ages were determined by timed mating with the day of the plug being embryonic day (E) 0.5. All the animal experiments were reviewed and approved by the University of Tokyo Animal Care and Use Committee.

3.2. Cell sorting

Kidneys were collected from E17.5 *Ednra*$^{EGFP/+}$ and wild-type embryos and dissected into pieces. Then the kidneys were incubated in D-MEM (Wako) containing 1 mg/ml of collagenase (Sigma) at 37 °C for 60 min. After disaggregated in 0.05% trypsin–EDTA solution (Sigma) to obtain single-cell suspensions, cells were subjected to hypotonic treatment for hemolyzation and resuspended in an appropriate volume of FACS buffer (5% fetal bovine serum/PBS). For cell sorting, the cells were passed through a cell strainer (BD Bioscience) and sorted into EGFP-positive and EGFP-negative cells using a FACS VantageSE flow cytometer (BD Bioscience). The data were analyzed with CellQuest software (BD Bioscience). For FACS analysis, the cells collected form wild-type embryos were lectin stained. The cells were incubated with FITC-conjugated lectin from *Bandeiraea simplicifolia* (BS-1) (Sigma), FITC-conjugated *Dolichos biflorus* agglutinin (DBA) (J-Oilmills), or biotin-conjugated *Lotus tetragonolobus* agglutinin (LTA) (Vector) on ice for 30 min. The cells incubated with biotin-conjugated

LTA were washed with an excess amount of FACS buffer, and incubated with PE-conjugated streptavidin (BD Bioscience) on ice for 30 min. The cells were washed and resuspended in FACS buffer again at an appropriate concentration, and passed through a cell strainer before FACS analysis. Analyses were performed on a FACS VantageSE flow cytometer, and data were analyzed with CellQuest software. In the assay, electronic gating was set to exclude nonviable cells with propidium iodide (PI) (Sigma) staining after cellular fractionation on the basis of forward versus side scatter.

3.3. RT-PCR

After cell sorting, EGFP-positive and EGFP-negative cells were subjected to conventional RT-PCR. Extraction of total RNA, reverse-transcription, and conventional PCR was performed as described previously with minor modifications (Asai et al., 2010). PCR on the resulting cDNA was performed using the primers 5′-GACGTAAACGGCCACAAGTTCA-3′ and 5′-GAACTCCAGCAGGACCA TGTGATC-3′ for *EGFP* (product size, 608 bp: annealing temperature, 65 °C), 5′-ACGCTGGCCTTTCG-3′ and 5′-CTGAGCAGTTCACA CCGGTTCTTATC-3′ for *Ednra* (product size, 603 bp: annealing temperature, 62 °C), 5′-CACAGTGCTGAGTCTTTGTGCTCT-3′ and 5′-ACCTATGGGTTCGGGGACAG-3′ for *Ednrb* (product size, 157 bp: annealing temperature, 60 °C), 5′-AGGACAGACCCTTCCACCAA-3′ and 5′-AATGACAACCACCGCAATGA-3′ for *CD31* (product size, 206 bp; annealing temperature, 62 °C), 5′-TGCCGAGCGTGAGAT TG-3′ and 5′-AATGAAAGATGGCTGGAAGAGAG-3′ for *αSMA* (product size, 193 bp; annealing temperature, 62 °C), 5′-GGCTATGTG-CAGTGTCATGTC-3′ and 5′-CTGTGATATGCCAGTGGTCAG-3′ for *Aqp1* (product size, 462 bp; annealing, 62 °C), 5′-ATCAAG CTGCCCATCTACAC-3′ and 5′-GGGCCAGCTTCACATTCTC-3′ for *Aqp3* (product size, 559 bp; annealing temperature, 60 °C), 5′-CCAGA-GAATTCCAGAGGGAAAGGT-3′ and 5′-CAGATACATCCACACCG TTTAGCGG-3′ for *GDNF* (product size, 338 bp; annealing temperature, 60 °C), 5′-ATCCCGCTCAAGAAAATGCC-3′ and 5′-TGTGTCA CAGTGATTCCACC-3′ for *Ren1* (product size, 416 bp: annealing temperature, 62 °C), 5′-GGTGTGAACCACGAGAAATAT-3′ and 5′-AGAT-CCACGACGGACACATT-3′ for *Gapdh* (product seize, 334 bp: annealing temperature, 60 °C).

3.4. β-Galactosidase staining

lacZ expression was detected by staining with X-Gal (5-bromo-4-chloro-3-indolyl β-D-galactoside) for β-galactosidase activity. Section staining was performed as described previously with minor modifications (Nagy et al., 2003). Sections were counterstained with 1% orange G (Sigma).

3.5. In situ hybridization

Sections (12 μm) were prepared from frozen mouse kidney samples. Treatment for in situ hybridization was as described with minor modifications (Ishii et al., 1997). The *Ednra* probe has been described previously (Sato et al., 2008a).

3.6. Immunohistochemistry

Immunohistochemistry of sections was performed as described previously with minor modifications (Makita et al., 2008). Embryo cryosections (12 μm) were immunostained using the following antibodies: rat monoclonal anti-GFP (Nacalai Tesque, Kyoto, Japan; 1:200), rabbit anti-GFP (Medical and Biological Laboratories, Nagoya, Japan; 1:250), rat anti-CD31 (BD Pharmingen, 1:200), mouse anti-αSMA (Sigma, 1:500), goat anti-Renin (Santa Cruz, 1:100). Signals were visualized with Rhodamine Red- or FITC-conjugated secondary antibodies specific for the appropriate species. When visualizing signals with anti-mouse secondary antibody, we used M.O.M. Blocking Reagent (Vector) to reduce background staining. Nuclei were visualized with TO-PRO-3 (Molecular Probes).

Acknowledgements

We also thank Yuko Fujisawa and Sakura Kushiyama for technical assistance. This work was supported in part by Global COE Program (Integrative Life Science Based on the Study of Biosignaling Mechanisms), MEXT, Japan, grants-in-aid for scientific research from the Ministry of Education, Culture, Sports, Science and Technology, Japan, grants-in-aid for scientific research from the Ministry of Health, Labour and Welfare of Japan.

Appendix A. Supplementary data

Supplementary data associated with this article can be found, in the online version, at doi:10.1016/j.gep.2011.04.001.

References

Ahn, D., Ge, Y., Stricklett, P.K., Gill, P., Taylor, D., Hughes, A.K., Yanagisawa, M., Miller, L., Nelson, R.D., Kohan, D.E., 2004. Collecting duct-specific knockout of endothelin-1 causes hypertension and sodium retention. J. Clin. Invest. 114, 504–511.

Asai, R., Kurihara, Y., Fujisawa, K., Sato, T., Kawamura, Y., Kokubo, H., Tonami, K., Nishiyama, K., Uchijima, Y., Miyagawa-Tomita, S., et al., 2010. Endothelin receptor type A expression defines a distinct cardiac subdomain within the heart field and is later implicated in chamber myocardium formation. Development (Cambridge, England) 137, 3823–3833.

Brochu, E., Lacasse, S., Moreau, C., Lebel, M., Kingma, I., Grose, J.H., Lariviere, R., 1999. Endothelin ET(A) receptor blockade prevents the progression of renal failure and hypertension in uraemic rats. Nephrol. Dial. Transplant. 14, 1881–1888.

Chow, L.H., Subramanian, S., Nuovo, G.J., Miller, F., Nord, E.P., 1995. Endothelin receptor mRNA expression in renal medulla identified by in situ RT-PCR. Am. J. Physiol. 269, F449–457.

Dhaun, N., Goddard, J., Webb, D.J., 2006. The endothelin system and its antagonism in chronic kidney disease. J. Am. Soc. Nephrol. 17, 943–955.

Gariepy, C.E., Ohuchi, T., Williams, S.C., Richardson, J.A., Yanagisawa, M., 2000. Salt-sensitive hypertension in endothelin-B receptor-deficient rats. J. Clin. Invest. 105, 925–933.

Hirata, Y., Matsuoka, H., Kimura, K., Fukui, K., Hayakawa, H., Suzuki, E., Sugimoto, T., Yanagisawa, M., Masaki, T., 1989. Renal vasoconstriction by the endothelial cell-derived peptide endothelin in spontaneously hypertensive rats. Circ. Res. 65, 1370–1379.

Honing, M.L., Hijmering, M.L., Ballard, D.E., Yang, Y.P., Padley, R.J., Morrison, P.J., Rabelink, T.J., 2000. Selective ET(A) receptor antagonism with ABT-627 attenuates all renal effects of endothelin in humans. J. Am. Soc. Nephrol. 11, 1498–1504.

Humphreys, B.D., Lin, S.L., Kobayashi, A., Hudson, T.E., Nowlin, B.T., Bonventre, J.V., Valerius, M.T., McMahon, A.P., Duffield, J.S., 2010. Fate tracing reveals the pericyte and not epithelial origin of myofibroblasts in kidney fibrosis. Am. J. Pathol. 176, 85–97.

Ishii, Y., Fukuda, K., Saiga, H., Matsushita, S., Yasugi, S., 1997. Early specification of intestinal epithelium in the chicken embryo: a study on the localization and regulation of CdxA expression. Dev. Growth Differ. 39, 643–653.

Kobayashi, A., Valerius, M.T., Mugford, J.W., Carroll, T.J., Self, M., Oliver, G., McMahon, A.P., 2008. Six2 defines and regulates a multipotent self-renewing nephron progenitor population throughout mammalian kidney development. Cell Stem Cell 3, 169–181.

Kurihara, H., Kurihara, Y., Nagai, R., Yazaki, Y., 1999. Endothelin and neural crest development. Cell. Mol. Biol. (Noisy-le-grand) 45, 639–651.

Kurihara, Y., Kurihara, H., Suzuki, H., Kodama, T., Maemura, K., Nagai, R., Oda, H., Kuwaki, T., Cao, W.H., Kamada, N., et al., 1994. Elevated blood pressure and craniofacial abnormalities in mice deficient in endothelin-1. Nature 368, 703–710.

Makita, R., Uchijima, Y., Nishiyama, K., Amano, T., Chen, Q., Takeuchi, T., Mitani, A., Nagase, T., Yatomi, Y., Aburatani, H., et al., 2008. Multiple renal cysts, urinary concentration defects, and pulmonary emphysematous changes in mice lacking TAZ. Am. J. Physiol. Renal. Physiol. 294, F542–553.

Maric, C., Ryan, G.B., Alcorn, D., 1997. Embryonic and postnatal development of the rat renal interstitium. Anat. Embryol. (Berl) 195, 503–514.

Masaki, T., 2004. Historical review: endothelin. Trends Pharmacol. Sci. 25, 219–224.

Matsumura, Y., Kuro, T., Kobayashi, Y., Konishi, F., Takaoka, M., Wessale, J.L., Opgenorth, T.J., Gariepy, C.E., Yanagisawa, M., 2000. Exaggerated vascular and renal pathology in endothelin-B receptor-deficient rats with deoxycorticosterone acetate–salt hypertension. Circulation 102, 2765–2773.

Matsushita, K., Morello, F., Wu, Y., Zhang, L., Iwanaga, S., Pratt, R.E., Dzau, V.J., 2010. Mesenchymal stem cells differentiate into renin-producing juxtaglomerular (JG)-like cells under the control of liver X receptor-alpha. J. Biol. Chem. 285, 11974–11982.

Nagy, A., Gertsenstein, M., Vintersten, K., Behringer, R., 2003. Manipulating the Mouse Embryo: A Laboratory Manual, 3rd ed. Cold Spring Harbor Laboratory Press.

Nangaku, M., Yamada, K., Gariepy, C.E., Miyata, T., Inagi, R., Kurokawa, K., Yanagisawa, M., Fujita, T., Johnson, R.J., 2002. ET(B) receptor protects the tubulointerstitium in experimental thrombotic microangiopathy. Kidney Int. 62, 922–928.

Owen, R.A., Molon-Noblot, S., Hubert, M.F., Kindt, M.V., Keenan, K.P., Eydelloth, R.S., 1995. The morphology of juxtaglomerular cell hyperplasia and hypertrophy in normotensive rats and monkeys given an angiotensin II receptor antagonist. Toxicol. Pathol. 23, 606–619.

Rakugi, H., Nakamaru, M., Saito, H., Higaki, J., Ogihara, T., 1988. Endothelin inhibits renin release from isolated rat glomeruli. Biochem. Biophys. Res. Commun. 155, 1244–1247.

Ryan, M.J., Black, T.A., Millard, S.L., Gross, K.W., Hajduczok, G., 2002. Endothelin-1 increases calcium and attenuates renin gene expression in As4.1 cells. Am. J. Physiol. Heart Circ. Physiol. 283, H2458–2465.

Sato, T., Kawamura, Y., Asai, R., Amano, T., Uchijima, Y., Dettlaff-Swiercz, D.A., Offermanns, S., Kurihara, Y., Kurihara, H., 2008a. Recombinase-mediated cassette exchange reveals the selective use of Gq/G11-dependent and -independent endothelin 1/endothelin type A receptor signaling in pharyngeal arch development. Development (Cambridge, England) 135, 755–765.

Sato, T., Kurihara, Y., Asai, R., Kawamura, Y., Tonami, K., Uchijima, Y., Heude, E., Ekker, M., Levi, G., Kurihara, H., 2008b. An endothelin-1 switch specifies maxillomandibular identity. Proc. Natl. Acad. Sci. USA 105, 18806–18811.

Sauter, A., Machura, K., Neubauer, B., Kurtz, A., Wagner, C., 2008. Development of renin expression in the mouse kidney. Kidney Int. 73, 43–51.

Sequeira Lopez, M.L., Pentz, E.S., Nomasa, T., Smithies, O., Gomez, R.A., 2004. Renin cells are precursors for multiple cell types that switch to the renin phenotype when homeostasis is threatened. Dev. Cell 6, 719–728.

Sequeira Lopez, M.L., Pentz, E.S., Robert, B., Abrahamson, D.R., Gomez, R.A., 2001. Embryonic origin and lineage of juxtaglomerular cells. Am. J. Physiol. Renal. Physiol. 281, F345–356.

Sorokin, A., Kohan, D.E., 2003. Physiology and pathology of endothelin-1 in renal mesangium. Am. J. Physiol. Renal. Physiol. 285, F579–589.

Terada, Y., Tomita, K., Nonoguchi, H., Marumo, F., 1992. Different localization of two types of endothelin receptor mRNA in microdissected rat nephron segments using reverse transcription and polymerase chain reaction assay. J. Clin. Invest. 90, 107–112.

Tomita, K., Nonoguchi, H., Terada, Y., Marumo, F., 1993. Effects of ET-1 on water and chloride transport in cortical collecting ducts of the rat. Am. J. Physiol. 264, F690–696.

Vainio, S., Lin, Y., 2002. Coordinating early kidney development: lessons from gene targeting. Nat. Rev. Genet. 3, 533–543.

Yanagisawa, M., Kurihara, H., Kimura, S., Tomobe, Y., Kobayashi, M., Mitsui, Y., Yazaki, Y., Goto, K., Masaki, T., 1988. A novel potent vasoconstrictor peptide produced by vascular endothelial cells. Nature 332, 411–415.

Fig. S1

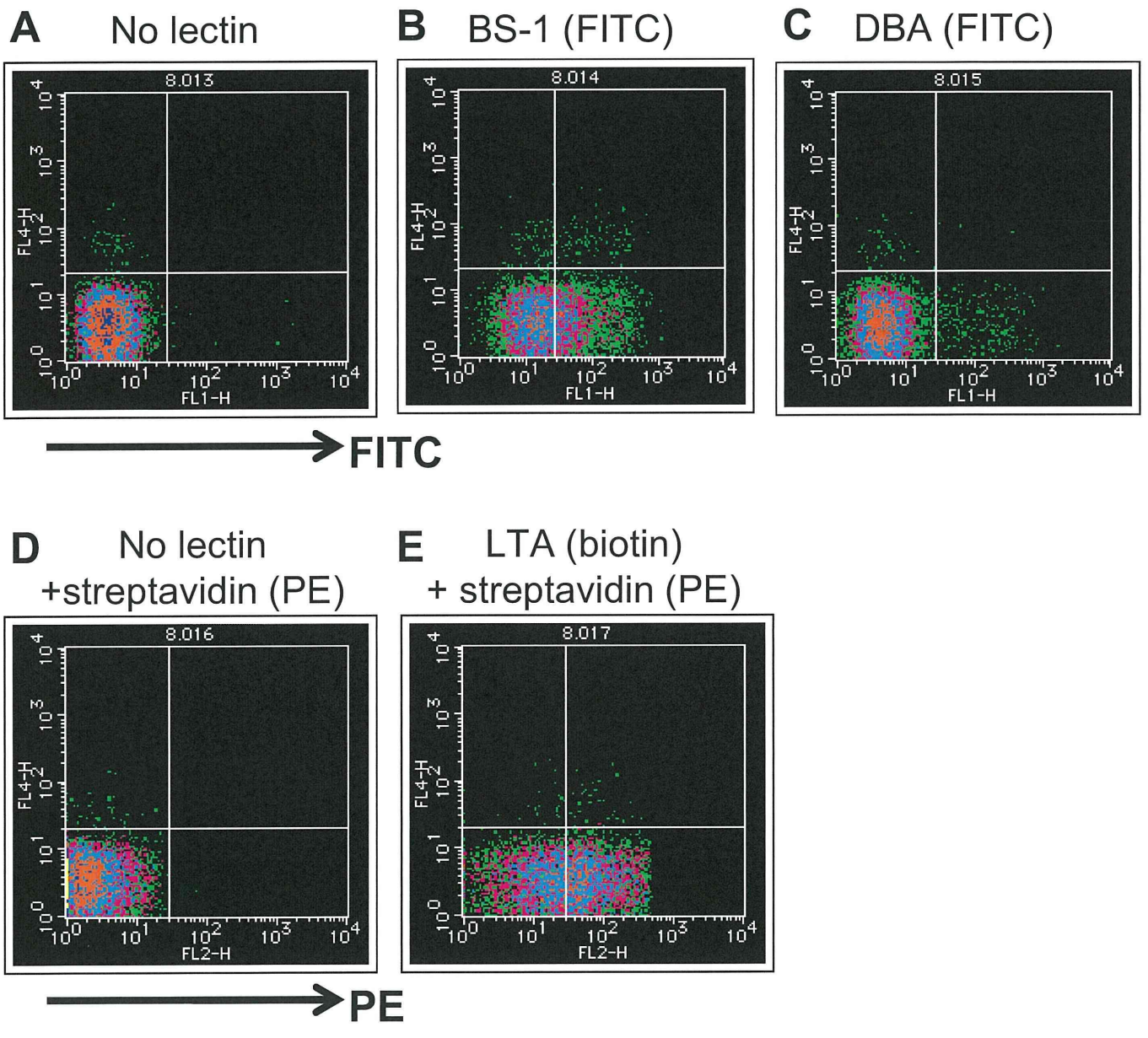
A No lectin
B BS-1 (FITC)
C DBA (FITC)
8.013
8.014
8.015
FL4-H
FL1-H
FITC
D No lectin
+streptavidin (PE)
E LTA (biotin)
+ streptavidin (PE)
8.016
8.017
FL2-H
PE

Fig. S2

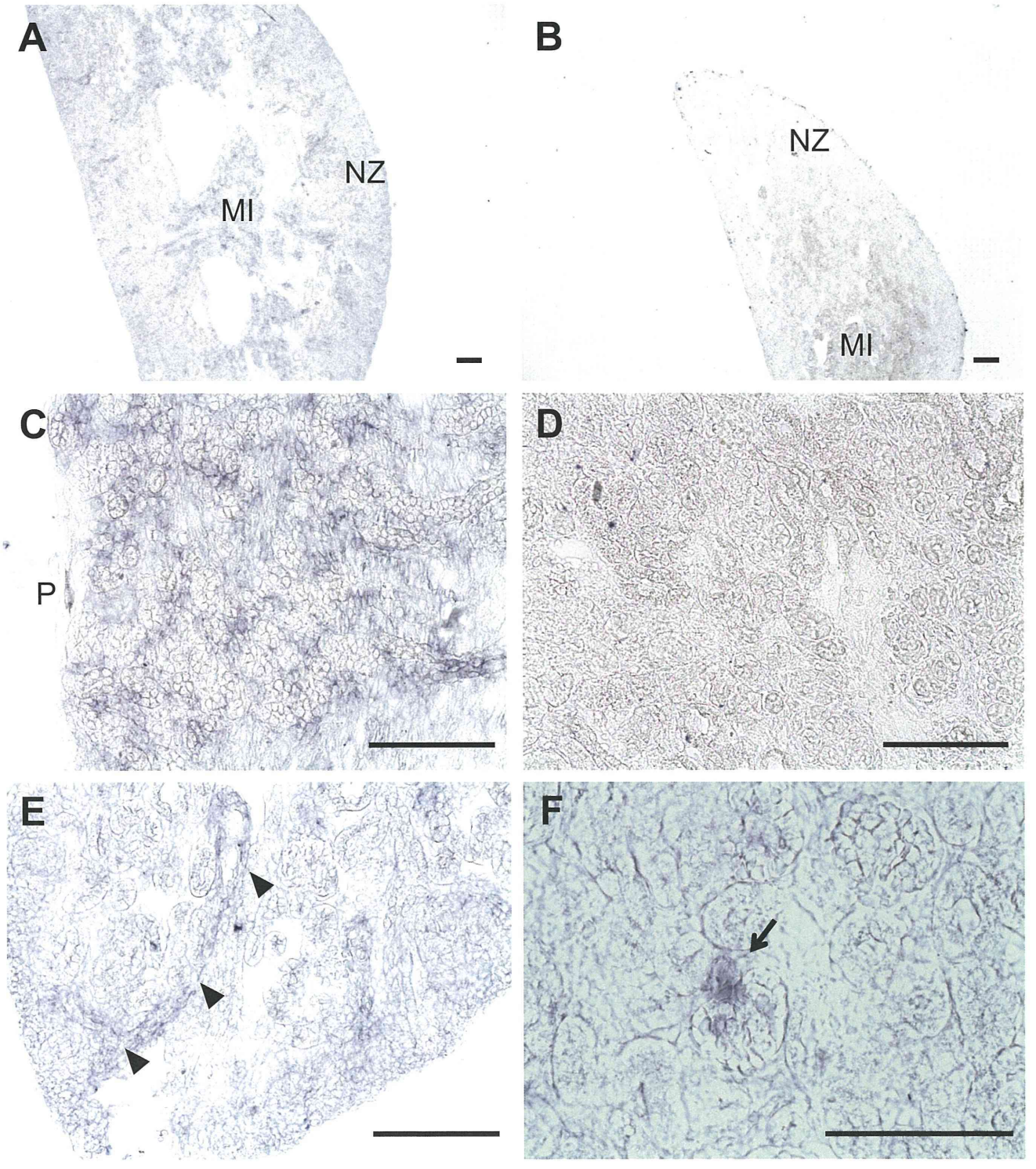

Calpain-6, a microtubule-stabilizing protein, regulates Rac1 activity and cell motility through interaction with GEF-H1

Kazuo Tonami[1,2], Yukiko Kurihara[1], Satoshi Arima[1], Koichi Nishiyama[1], Yasunobu Uchijima[1], Tomoichiro Asano[3], Hiroyuki Sorimachi[2] and Hiroki Kurihara[1,*]

[1]Department of Physiological Chemistry and Metabolism, Graduate School of Medicine, The University of Tokyo, 7-3-1 Hongo, Bunkyo-ku, Tokyo 113-0033, Japan
[2]Calpain Project, The Tokyo Metropolitan Institute of Medical Science (Rinshoken), 2-1-6 Kamikitazawa, Setagaya-ku, Tokyo 156-8506, Japan
[3]Department of Biomedical Chemistry, Hiroshima University Graduate School of Biomedical Sciences, Kasumi 1-2-3, Hiroshima 734-8551, Japan
*Author for correspondence (kuri-tky@umin.ac.jp)

Accepted 2 December 2010
Journal of Cell Science 124, 1214-1223

doi:10.1242/jcs.072561

Summary

Crosstalk between microtubules and actin filaments is crucial for various cellular functions, including cell migration, spreading and cytokinesis. The Rac1 GTPase plays a key role in such crosstalk at the leading edge of migrating cells in order to promote lamellipodial formation. However, the mechanism underlying the link between microtubules and Rac1 activation remains unclear. Here, we show that calpain-6 (CAPN6), a non-proteolytic calpain with microtubule-binding and -stabilizing activity, might participate in this crosstalk. Small interfering RNA (siRNA)-induced knockdown of *Capn6* in NIH 3T3 cells resulted in Rac1 activation, which promoted cell migration, spreading and lamellipodial protrusion. This increase in Rac1 activity was abolished by knockdown of the Rho guanine nucleotide exchange factor *GEF-H1* (officially known as *Arhgef2*). CAPN6 and GEF-H1 colocalized with microtubules and also interacted with each other through specific domains. Upon knockdown of *Capn6*, GEF-H1 was shown to translocate from microtubules to the lamellipodial region and to interact with Rac1. By contrast, RhoA activity was decreased upon knockdown of *Capn6*, although low levels of active RhoA or the presence of RhoA molecules appeared to be required for the *Capn6*-knockdown-induced Rac1 activation. We suggest that CAPN6 acts as a potential regulator of Rac1 activity, through a mechanism involving interaction with GEF-H1, to control lamellipodial formation and cell motility.

Key words: Actin, Calpain, Cell motility, Microtubule, Rac1

Introduction

Crosstalk between the two major cytoskeletal components, actin filaments and microtubules, is essential for various cellular functions, including cell migration, spreading and cytokinesis. In migrating cells, actin polymerization generates lamellipodial membrane protrusions at the leading edge, and actomyosin contractility in the tail promotes cell-body advancement (Chhabra and Higgs, 2007). In concert with the actin cytoskeleton, the dynamics of microtubules contributes to the establishment of cell polarity and the directional movement of migrating cells. The initial polarization of microtubule assembly is led by actin filaments, and conversely the polarized microtubules contribute to the reorganization of actin filaments (Li and Gundersen, 2008; Rodriguez et al., 2003; Siegrist and Doe, 2007).

Rho family GTPases and their regulatory proteins have been postulated to play central roles in microtubule–actin crosstalk. Microtubule depolymerization, by nocodazole or colchicine, induces Rho activation with an increase in stress fiber formation and cellular contractility (Enomoto, 1996; Ren et al., 1999). This effect is mediated by the Rho guanine-nucleotide-exchange factor GEF-H1 (officially known as ARHGEF2), which is released from microtubules upon depolymerization (Chang et al., 2008; Krendel et al., 2002). By contrast, microtubular growth after washout of nocodazole activates Rac1, leading to actin polymerization in lamellipodial protrusions (Waterman-Storer et al., 1999). Although GEF-H1 has been suggested as a potential mediator of microtubule–actin crosstalk at the leading edge (Siegrist and Doe, 2007; Waterman-Storer et al., 1999), this has not been proven. GEF-H1 was originally reported to be a GEF for both RhoA and Rac1 (Ren et al., 1998), but subsequent reports have not demonstrated a GEF activity for Rac1 (Benais-Pont et al., 2003; Glaven et al., 1999; Krendel et al., 2002; Zenke et al., 2004). Thus, the effect of GEF-H1 on Rac1 activity might depend upon the presence or absence of regulatory factors (Birkenfeld et al., 2008). A recent report has demonstrated that GEF-H1 can promote Rac1 activation in the presence of the p21-activated kinase PAK4 (Callow et al., 2005), indicating that the activation of Rac1 by GEF-H1 might be conditionally regulated.

The calpains are a family of intracellular cysteine proteases whose activity is highly dependent upon Ca^{2+} ions (Croall and Ersfeld, 2007; Goll et al., 2003; Hanna et al., 2008). Approximately one-half of calpains share a common four-domain structure comprising domains I to IV: domain II is a cysteine protease domain; domain III is related to the C2 domain, a Ca^{2+}- and phospholipid-binding module; and domain IV is characterized by the presence of multiple EF-hand motifs in some members, including the classical calpains (m- and μ-calpains) (Croall and Ersfeld, 2007; Goll et al., 2003). Among the 14 or 15 members of the calpain family in mammals, calpain-6 (CAPN6) is unique in that it lacks the active-site catalytic cysteine residue and is therefore

not likely to be a proteolytic enzyme (Dear et al., 1997). In CAPN6, as well as Capn5, the C-terminal structure is defined as a diverged C2-domain (also called domain T) instead of as domain IV, on the basis of similarity to *Caenorhabditis elegans* TRA-3, a nematode sex determination factor (Barnes and Hodgkin, 1996; Dear et al., 1997; Goll et al., 2003; Mugita et al., 1997). Recently, we have demonstrated that CAPN6 can bind to microtubules, mainly through domain III, and induce microtubule stabilization through non-proteolytic activity (Tonami et al., 2007). Furthermore, inactivation of CAPN6 not only destabilizes microtubules but also promotes formation of lamellipodia and lamellipodial membrane ruffling (Tonami et al., 2007). These findings have led us to study the possibility that CAPN6 participates in microtubule–actin crosstalk in order to contribute to cellular functions. Here, we demonstrate that CAPN6 is a possible mediator of microtubule–actin crosstalk. RNA interference (RNAi)-induced knockdown revealed that CAPN6 suppresses Rac1 activity and lamellipodial formation, in a manner related to changes in microtubule dynamics, through interaction with GEF-H1. Biochemical and immunocytochemical experiments showed that there was a direct association between CAPN6 and GEF-H1. These results might provide a clue to previously unknown regulatory mechanisms that underlie microtubule–actin crosstalk in lamellipodial formation and cell motility.

Results

Knockdown of *Capn6* promotes cell motility and spreading, with enhancement of lamellipodial membrane ruffling

To investigate the function of CAPN6 in cell motility, we performed Boyden chamber migration assays and scratch-wound-healing assays on NIH 3T3 cells transfected with small interfering RNA (siRNA) targeting *Capn6* or with control siRNA. We designed two independent siRNAs for *Capn6* (*Capn6*-1 and *Capn6*-2), both of which successfully downregulated CAPN6 protein levels (Fig. 1A). In the Boyden chamber assay, knockdown of *Capn6* caused a marked enhancement in the three-dimensional migration of the cells in response to platelet-derived growth factor (PDGF)-BB (Fig. 1B). Consistent with this observation are the results of in vitro wound-healing assays, which showed that, upon knockdown

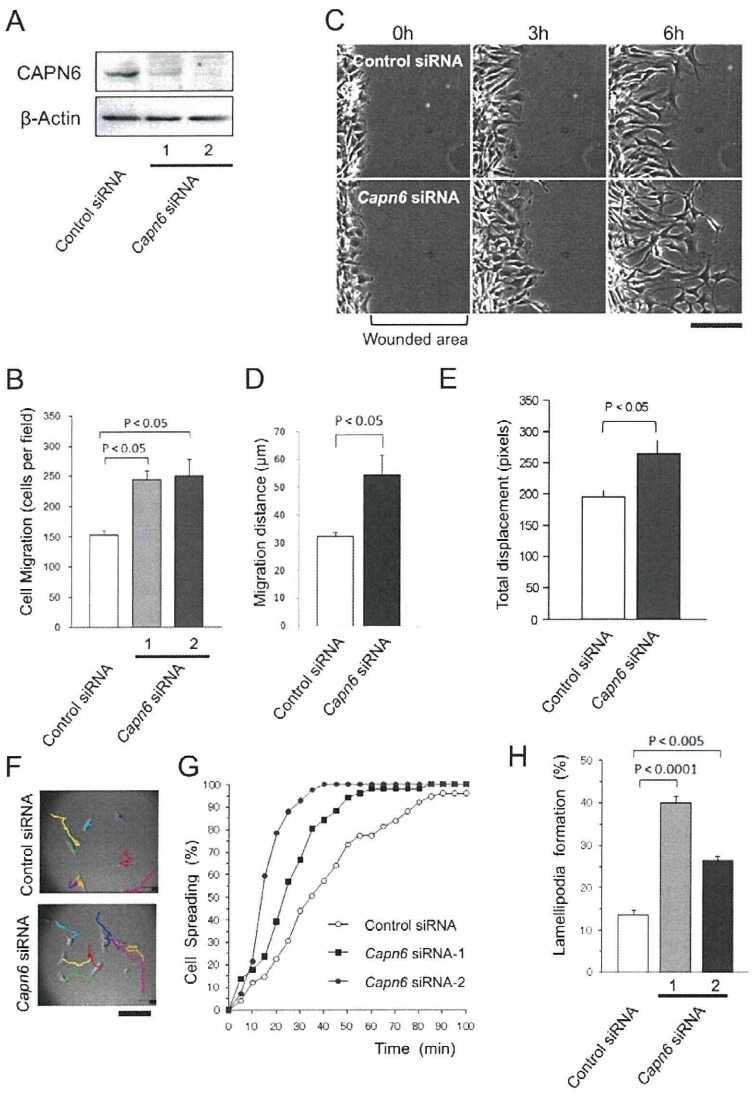

Fig. 1. Effects of siRNA-induced CAPN6 knockdown on cell migration, spreading and lamellipodial membrane ruffling in NIH 3T3 cells. (**A**) Confirmation of CAPN6 knockdown by western blotting with an anti-CAPN6 C-terminus antibody. Stealth siRNAs targeting two different regions of the *Capn6* transcript (1 and 2 for nucleotides 1518–1542 and 1935–1959, respectively) downregulated CAPN6 protein levels. (**B**) Three-dimensional migration assay. The Boyden chamber assay was performed with a type IV collagen-coated polycarbonate filter (5 μg filter) (means±s.e.m.; n=3; Scheffe's test). (**C**) Two-dimensional scratch wound assay. A monolayer of NIH 3T3 cells, transfected with siRNA, was wounded and evaluated for migration. Many lamellipodial protrusions extended into the wounded space, and membrane ruffling and enhanced migration were observed in *Capn6* siRNA-transfected cells. Scale bar: 50 μm. (**D**) Quantification of the distance of cell migration into the wounded area. The migration distance in each experiment was determined as the mean of the migration distances of ten cells (means±s.e.m.; n=3; Student's t-test). (**E**,**F**) Random migration assay. The total displacement was calculated using the tracks of 3–8 cells in each experiment (means±s.e.m.; n=4; Mann–Whitney U-test). The tracks of migration of NIH 3T3 cells transfected with siRNA were recorded in time-lapse movies at 5-minute intervals for 4 hours. Scale bar: 100 μm. (**G**) Cell spreading assay. Cells were visualized by phase-contrast microscopy and scored for the percentage of spread cells at the indicated times. (**H**) Comparison of the numbers of cells with lamellipodia. Random fields of the cells were photographed, and 100 cells exhibiting fluorescence were examined. Cells exhibiting clearly discernible lamellipodia or membrane ruffles (>10 μm in width) were scored as positive (means±s.e.m.; n=3; Scheffe's test).

of *Capn6*, cells exhibited extensive lamellipodia formation at the leading edge and a significant increase in the migration distance compared with that of control siRNA-treated cells (Fig. 1C,D). Enhanced cell movement upon knockdown of *Capn6* was further confirmed by cell tracking in the random migration assay (Fig. 1E,F). We also examined whether CAPN6 was involved in cell spreading, which shares common mechanisms regulating cytoskeletal organization with those in cell migration (Huveneers and Danen, 2009). For the evaluation of spreading, cells were induced to round up (but not detach) by brief trypsinization and were allowed to re-spread for 2 hours. Knockdown of *Capn6* significantly promoted re-spreading of rounded cells (Fig. 1G; supplementary material Fig. S1).

Promotion of cell migration and spreading in cells upon knockdown of *Capn6* was accompanied by activation of lamellipodial protrusion and membrane ruffling at the cell edges (Fig. 1H, supplementary material Fig. S2A), as previously described (Tonami et al., 2007). Although these effects are unlikely to be due to an siRNA-induced inhibition of proteolytic activity, because CAPN6 lacks the active-site catalytic cysteine residue, they might be due to derepression of other calpains that are 'blocked' by CAPN6. However, the lamellipodial formation induced by knockdown of *Capn6* was not affected by treatment with the calpain inhibitors benzyloxycarbonyl-L-leucyl-L-leucinal (ZLLal) or calpeptin (supplementary material Fig. S2B). These findings suggest that CAPN6 is involved in the regulation of the organization of cortical actin and subsequent changes in cell motility and morphology, independent of the proteolytic activity of calpains.

Rac1 activation is involved in the enhancement of cell motility and lamellipodial protrusion observed upon knockdown of *Capn6*

The enhancement of lamellipodial formation and cell motility described above led us to speculate that Rac1 is activated upon knockdown of *Capn6*. We therefore estimated Rac1 activity by measuring the levels of active GTP-bound Rac1 using a pull-down assay with PAK1-PBD (the PAK1 p21-binding domain) coated beads. As expected, Rac1 activity was upregulated upon knockdown of *Capn6*, whereas the total amount of Rac1 was unchanged (Fig. 2A,B). The *Capn6*-siRNA-induced Rac1 activation was not affected by ZLLal (supplementary material Fig. S2C), as in the case of lamellipodial protrusion. Conversely, overexpression of CAPN6 decreased the amount of Rac1-GTP, although the efficiency was different between the two CAPN6 fusion proteins (GFP–CAPN6 and CAPN6–Myc) (Fig. 2C), indicating that CAPN6 might act as a repressor of Rac1 activity. To test whether increased Rac1 activity was responsible for the effect of *Capn6* knockdown, we designed siRNAs targeting *Rac1*. The efficiency of the *Rac1*-siRNAs was confirmed by western blotting using a mouse polyclonal anti-Rac1 antibody (Fig. 2D). Co-transfection of *Rac1*- and *Capn6*-siRNA significantly suppressed the enhancement of cell motility and lamellipodial protrusions induced by knockdown of CAPN6 (Fig. 2E,F; supplementary material Fig. S3A). We also tested whether the effect of *Rac1*-siRNA was reproduced upon treatment of cells with the Rac1 inhibitor NSC23766. As expected, NSC23766 effectively suppressed the enhancement of lamellipodia and cell motility caused by *Capn6*-siRNA (Fig. 2G,H; supplementary material Fig. S3B). These results show that Rac1 activity is involved in the lamellipodial formation and enhanced cell motility that is induced by knockdown of CAPN6.

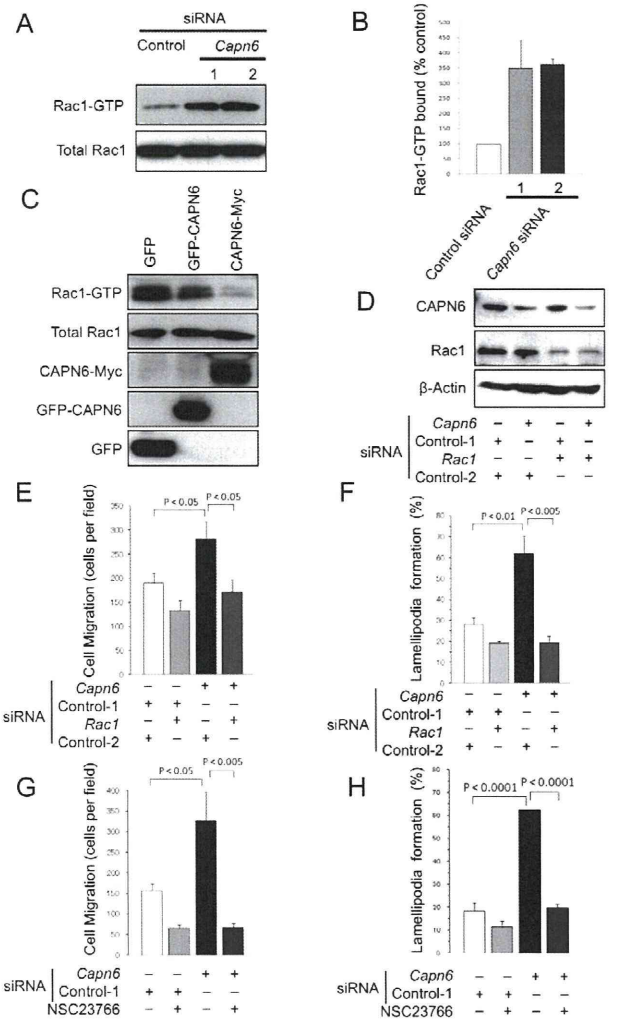

Fig. 2. Involvement of Rac1 in *Capn6* siRNA-induced enhancement of cell motility and lamellipodial protrusion. (**A**) Rac1 activation upon *Capn6* knockdown. A representative immunoblot of precipitated GTP-bound Rac1 from cell lysates, probed with the anti-Rac1 antibody. At 48 hours after siRNA transfection, the conditioned medium was replaced with serum-free medium and cells were cultured for an additional 18 hours. (**B**) Quantification of the relative amounts of Rac1-GTP in control cells and in cells upon knockdown of *Capn6* (means±s.e.m.; n=3). (**C**) Rac1 inactivation by CAPN6 overexpression. Lysates were prepared from serum-fed cells at 18 hours after transfection with expression vectors encoding GFP, GFP–CAPN6 and CAPN6–Myc. (**D**) siRNA-induced CAPN6 and Rac1 knockdown was confirmed by western blotting at 48 hours after siRNA transfection. (**E–H**) Quantitative analysis of cell migration and lamellipodial formation. *Rac1* siRNA (E,F) and Rac1 inhibitor (50 μM NSC23766) (G,H) suppress the enhancement of cell migration in the Boyden chamber assay (E,G) and suppress the lamellipodial protrusion (F,H) induced by *Capn6* siRNA [means±s.e.m.; n=3; Fisher's test (E,G) and Scheffe's test (F,H)].

GEF-H1 mediates Rac1 activation induced by knockdown of *Capn6*

To explore the link between CAPN6 and Rac1, we focused on GEF-H1, which is known to be associated with microtubules, as is CAPN6. Signals for endogenous CAPN6 and GEF-H1 were partially

overlapped within the cytoplasm and were observed in a reticular pattern (Fig. 3A). The specificity of staining for CAPN6 and GEF-H1 and their colocalization to microtubules was confirmed by immunostaining after siRNA knockdown, together with western blotting for GEF-H1 (supplementary material Figs S4, S5). To test whether GEF-H1 could activate Rac1, we transfected a GEF-H1–His_6 expression vector into control cells and cells subjected to siRNA knockdown of *Capn6*. GEF-H1 overexpression increased Rac1 activity both in the control cells and in cells with *Capn6* knockdown (Fig. 3B). When each of the two siRNAs targeting *GEF-H1* (*Gef-h1*-1 and *Gef-h1*-2) was introduced into *Capn6*-knockdown cells, it significantly suppressed the Rac1 activation induced by *Capn6* siRNA (Fig. 3C,D). Furthermore, knockdown of *GEF-H1* plus *Capn6* suppressed the enhancement of cell migration and lamellipodial protrusions (Fig. 3E,F; supplementary material Fig. S6). *GEF-H1* knockdown appeared to decrease slightly the amount of GTP-Rac1 under serum-free conditions (Fig. 3C,D), but this effect was marginal. *GEF-H1* knockdown did not affect Rac1 activity in PDGF-stimulated cells (data not shown), indicating that GEF-H1 is not involved in PDGF-induced Rac1 activation. These results suggest that GEF-H1 is involved in the Rac1 activation induced by knockdown of CAPN6.

CAPN6 promotes microtubular association of GEF-H1 and prevents it from activating Rac1-mediated microtubule–actin crosstalk

To examine the effect of *Capn6* knockdown on the intracellular behavior of GEF-H1, we stained control and *Capn6*-knockdown cells for endogenous GEF-H1 and compared its localization with the distribution of microtubules and actin filaments. In control siRNA-treated cells, GEF-H1 was largely colocalized to microtubules (Fig. 4A,B; supplementary material Fig. S7). However, upon knockdown of *Capn6*, GEF-H1 appeared to re-distribute from microtubules into the lamellipodial region (Fig. 4C,D; supplementary material Fig. S7), where it colocalized with peripheral actin filaments (Fig. 4E–H). By contrast, such translocation of GEF-H1 was hardly ever observed in lamellipodia induced by PDGF stimulation (supplementary material Fig. S8).

To confirm further the behavior of GEF-H1, we overexpressed GEF-H1–His_6 in control cells and in cells subjected to *Capn6* knockdown. GEF-H1–His_6 also changed its distribution pattern, re-distributing from microtubules into the lamellipodial region upon *Capn6* knockdown (Fig. 4I–L), which led to the colocalization of GEF-H1 with lamellipodial actin filaments (Fig. 4M–P). These observations indicate that GEF-H1 is readily mobilized from the

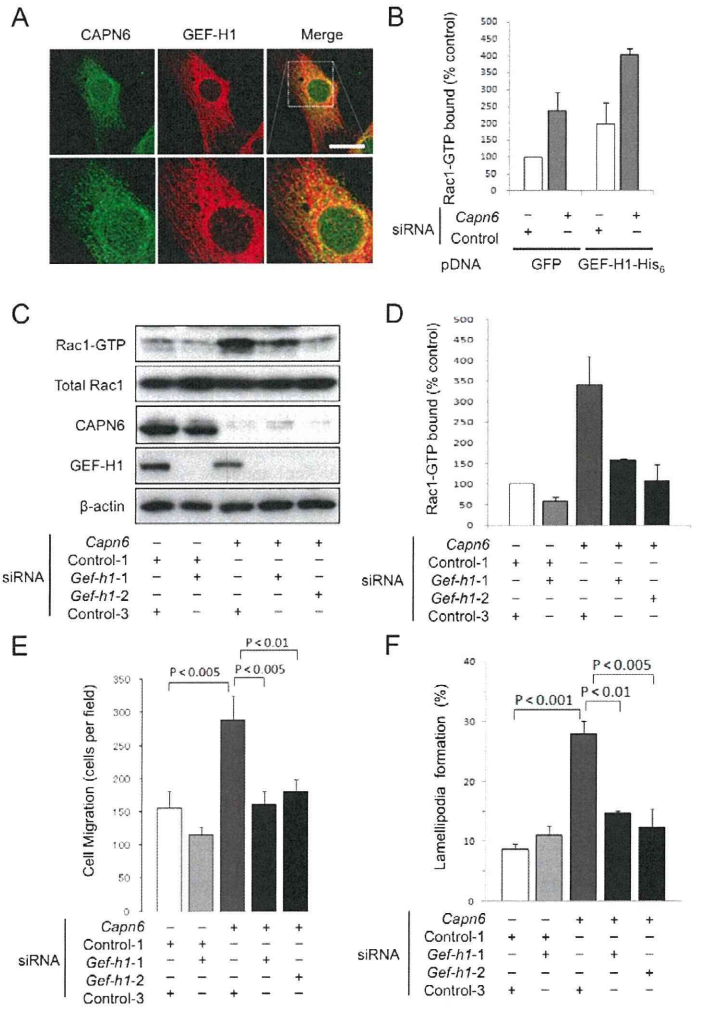

Fig. 3. Involvement of GEF-H1 in *Capn6*-siRNA-induced Rac1 activation. (**A**) Immunostaining for endogenous CAPN6 and GEF-H1 with antibodies against CAPN6 (domain II) and GEF-H1, respectively. CAPN6 partially colocalizes with GEF-H1. Scale bar: 20 μm. (**B**) Quantification of the relative amounts of Rac1-GTP in cells (control and *Capn6* knockdown) co-transfected with GFP or His_6-tagged GEF-H1 vector (means±s.e.m.; n=3). (**C**) *GEF-H1* siRNA suppressed the Rac1 activation induced by *Capn6* knockdown. *Gef-h1*-1 and *Gef-h1*-2 siRNAs target two different regions of *GEF-H1* transcript. Successful gene knockdown was confirmed by western blotting with the anti-GEF-H1 antibody at 48 hours after siRNA transfection. (**D**) The relative amounts of Rac1-GTP (means±s.e.m.; n=3). (**E**,**F**) GEF-H1 knockdown suppressed the enhancement of cell motility in the Boyden chamber assay (E) and suppressed the lamellipodial protrusion (F) induced by *Capn6* siRNA [means±s.e.m.; n=3; Fisher's test (E) and Scheffe's test (F)].

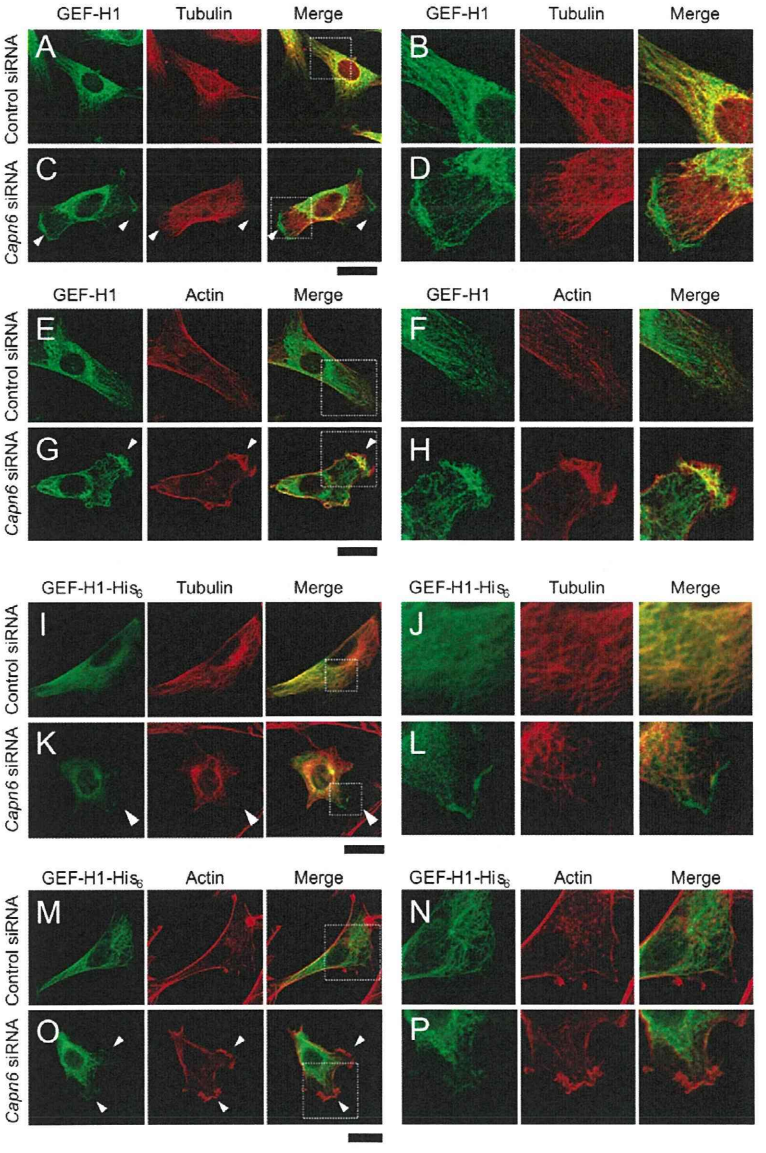

Fig. 4. GEF-H1 translocates from microtubules to the lamellipodial region upon knockdown of *Capn6*. (**A–D**) Immunostaining for endogenous GEF-H1 and tubulin in control (A,B) and *Capn6* (C,D) siRNA-transfected cells. In control cells, GEF-H1 is colocalized with microtubules. In *Capn6*-siRNA-transfected cells, GEF-H1 appears to distribute diffusely within the cytoplasm and partly translocates to lamellipodia (arrowheads). (**E–H**) Immunostaining for endogenous GEF-H1 and rhodamine–phalloidin staining for actin filaments in control (E,F) and *Capn6* (G,H) siRNA-transfected cells. In *Capn6*-siRNA-transfected cells, GEF-H1 appears to colocalize with the peripheral actin filaments in lamellipodia (arrowheads). (**I–L**) Immunostaining for GEF-H1–His_6 and tubulin in control (I,J) and *Capn6* (K,L) siRNA-transfected cells. In control cells, GEF-H1–His_6 is colocalized with microtubules. In *Capn6*-siRNA-transfected cells, GEF-H1 appears to distribute diffusely within the cytoplasm and to partly translocate to lamellipodia (arrowheads). (**M–P**) Immunostaining for GEF-H1–His_6 and rhodamine–phalloidin staining for actin filaments in control (M,N) and *Capn6* (O,P) siRNA-transfected cells. In *Capn6*-siRNA-transfected cells, GEF-H1 appears to colocalize with the peripheral actin filaments in lamellipodia (arrowheads). The boxed areas in A, C, E, G, I, K, M and O are enlarged in B, D, F, H, J, L, N and P, respectively. Scale bars: 20 μm.

microtubule network to peripheral actin filaments in the absence of CAPN6.

We investigated further whether CAPN6 regulates the interaction between GEF-H1 and microtubules. Cell lysates from control or *Capn6*-siRNA-transfected NIH 3T3 cells were subjected to a microtubule co-sedimentation assay. Co-sedimentation of both GEF-H1 and CAPN6 in the microtubule-containing pellet was intensified in the presence of paclitaxel, a microtubule-stabilizing agent (Fig. 5A). In *Capn6*-siRNA-transfected cells, the relative amount of GEF-H1 associated with microtubules was significantly decreased (Fig. 5A,B). In this assay, the total amount of microtubules sedimented (stabilized microtubules) was the same in control and *Capn6*-siRNA-treated cell lysates when in the presence of paclitaxel (Fig. 5A), indicating that the amount of GEF-H1 binding to microtubules was decreased in the absence of CAPN6. Furthermore, GEF-H1 was co-precipitated with the Rac1-GTP complex from cell lysates from *Capn6*-knockdown cells in a Rac1-activity assay (Fig. 5C). These results suggest that CAPN6 promotes GEF-H1–microtubule association and prevents GEF-H1 from activating Rac1-mediated microtubule–actin crosstalk.

CAPN6 physically interacts with GEF-H1

Next, we overexpressed Myc-tagged CAPN6 and His_6-tagged GEF-H1 in NIH 3T3 cells to test whether CAPN6 might physically interact with GEF-H1 in vivo. GEF-H1–His_6 was detected in the immunoprecipitate from the anti-Myc antibody (Fig. 6A). We further examined whether endogenous CAPN6 and GEF-H1 associated with each other. As expected, GEF-H1 was co-precipitated with CAPN6 (i.e. it was detected with immunoprecipitates from the anti-CAPN6 antibody) (Fig. 6B). This association between CAPN6 and GEF-H1 in vivo was not affected by treatment with nocodazole (supplementary material Fig. S9), suggesting that this association is independent of microtubules. To examine whether CAPN6 and GEF-H1 could directly interact with each other and, if so, which domain was involved, we performed a GST pull-down assay using various GST–CAPN6 mutants coexpressed with GEF-H1–His_6

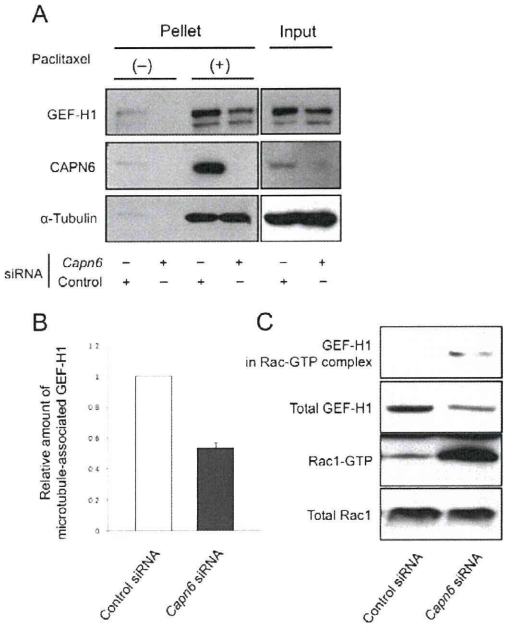

Fig. 5. Effects of siRNA-induced CAPN6 knockdown on the association of GEF-H1 with microtubules and active Rac1. (**A**,**B**) Microtubule co-sedimentation assay. (A) The western blot shows that GEF-H1 co-sediments with the microtubule pellets in the absence (–) and presence (+) of 20 μM paclitaxel in NIH 3T3 cells. (B) The amounts of microtubule-associated GEF-H1 relative to those of α-tubulin are decreased in *Capn6*-siRNA-transfected cells compared with that in control-siRNA-transfected cells. Data are normalized to the value of control-siRNA-transfected cells (means±s.e.m.; n=3). (**C**) Association of GEF-H1 with active Rac1 in *Capn6*-siRNA-transfected cells. The amounts of GEF-H1 co-precipitated with Rac1-GTP pulled down with PAK1-PBD-conjugated beads were increased in *Capn6*-siRNA-transfected cells compared with that in control-siRNA-transfected cells.

protein in NIH 3T3 cells (Fig. 6C). GEF-H1–His_6 was pulled down by GST-fused full-length CAPN6 and the CAPN6 domains II, III and T (Fig. 6C). We also found that the precipitates from the GST-fused full-length CAPN6 and the CAPN6 domains III and T contained β-tubulin (Fig. 6C), indicating that β-tubulin might mediate the pull-down of GEF-H1–His_6. This possibility is supported by our previous finding that CAPN6 binds to microtubules through domain III and domain T (Tonami et al., 2007). By contrast, β-tubulin was not detected in the precipitate of GST-fused CAPN6 domain II (Fig. 6C). The same result was reproduced by using in-vitro-translated GEF-H1–His_6 protein (data not shown). To determine which domain(s) of GEF-H1 were responsible for the interaction with CAPN6 domain II, we performed GST pull-down assays using GST-fused CAPN6 domain II and in-vitro-translated GEF-H1 derivatives (Fig. 6D). This mapped the association between GEF-H1 and CAPN6 domain II to the zinc-finger-containing N-terminal region (amino acids 1–240) of GEF-H1 (Fig. 6D). These results suggest that CAPN6 and GEF-H1 directly interact, most probably through domain II and the zinc-finger-containing N-terminal region, respectively.

Knockdown of *Capn6* suppresses RhoA activity

It is well known that GEF-H1 is a RhoA GEF and increases RhoA activity when it is released from microtubules (Birkenfeld et al., 2008; Chang et al., 2008; Krendel et al., 2002). Therefore, we examined whether RhoA activity might be increased upon knockdown of CAPN6. Unexpectedly, RhoA activity was largely decreased in cells upon *Capn6* knockdown (Fig. 7A). This effect was also seen upon treatment with NSC23766 (Fig. 7B), indicating that the decrease in RhoA activity was not due to Rac1 activation. It has been suggested recently that RhoA inactivation might increase Rac1 activity because RhoA suppresses Rac1 through a Rho-associated protein kinase (ROCK)-dependent mechanism (Narumiya et al., 2009). To test this possibility, we compared the contribution of GEF-H1 in Rac1 activation between cells upon *Capn6* knockdown and cells treated with Y-27632, a ROCK inhibitor. We found that the Y-27632-induced lamellipodial formation was not suppressed by *Gef-h1*-siRNA (supplementary material Fig. S10). Lamellipodial translocation of GEF-H1 was not observed in Y-27632-treated cells (supplementary material Fig. S8), indicating that GEF-H1-dependent Rac1 activation upon *Capn6* knockdown is not likely to be due to ROCK inactivation. Interestingly, *Capn6*-knockdown-induced Rac1 activation was not observed upon co-transfection of *RhoA* siRNA (Fig. 7C), but was still apparent upon treatment of cells with Y-27632 (supplementary material Fig. S11A). The lamellipodial formation induced by *Capn6* siRNA was also insensitive to Y-27632 (supplementary material Fig. S11B). Taken together, these results suggest that knockdown of CAPN6 causes suppression of RhoA activity independently of Rac1 activity, but that a ROCK-independent activity of RhoA or the presence of RhoA molecules, even if they are not activated, is necessary for GEF-H1-mediated Rac1 activation.

Capn6 expression is suppressed by serum

To investigate the physiological relevance of the GEF-H1-mediated Rac1 activity induced by the knockdown of CAPN6, we searched for factors that could affect CAPN6 expression. Notably, we found that *Capn6* mRNA and CAPN6 protein levels were downregulated by serum (Fig. 8A,B). To confirm the suppressive effect of serum on *Capn6* expression, we stimulated NIH 3T3 cells with fetal calf serum (FCS) for the indicated times after a 12-hour starvation. We found that *Capn6* mRNA levels were decreased by the addition of 10% FCS, in a time-dependent manner (Fig. 8C), and that this was accompanied by a decrease in CAPN6 protein levels (Fig. 8D). These results suggest that CAPN6–GEF-H1–Rac1 signaling might be regulated by serum-derived factor(s).

Discussion

In the present study, we characterize CAPN6, a non-proteolytic calpain that is associated with microtubules, as a regulator of Rac1-mediated lamellipodial formation and cell motility. siRNA-mediated *Capn6* knockdown resulted in Rac1 activation and subsequent enhancement of lamellipodial formation and cell motility. This *Capn6*-knockdown-induced Rac1 activation was dependent on GEF-H1. Biochemical evidence indicated that there was a direct interaction between CAPN6 and GEF-H1 through specific domains. In the absence of CAPN6 activity, GEF-H1 appears to be dissociated from the microtubules and translocated to the cortical actin network, where lamellipodial formation is upregulated. CAPN6 expression was downregulated by serum, which activates Rac1 and cell motility, suggesting that the CAPN6–GEF-H1–Rac1 regulatory pathway might contribute to the serum-dependent control of cell motility.

CAPN6 is a unique member of the calpain family – one of the crucial catalytic cysteine residues is replaced with lysine in humans

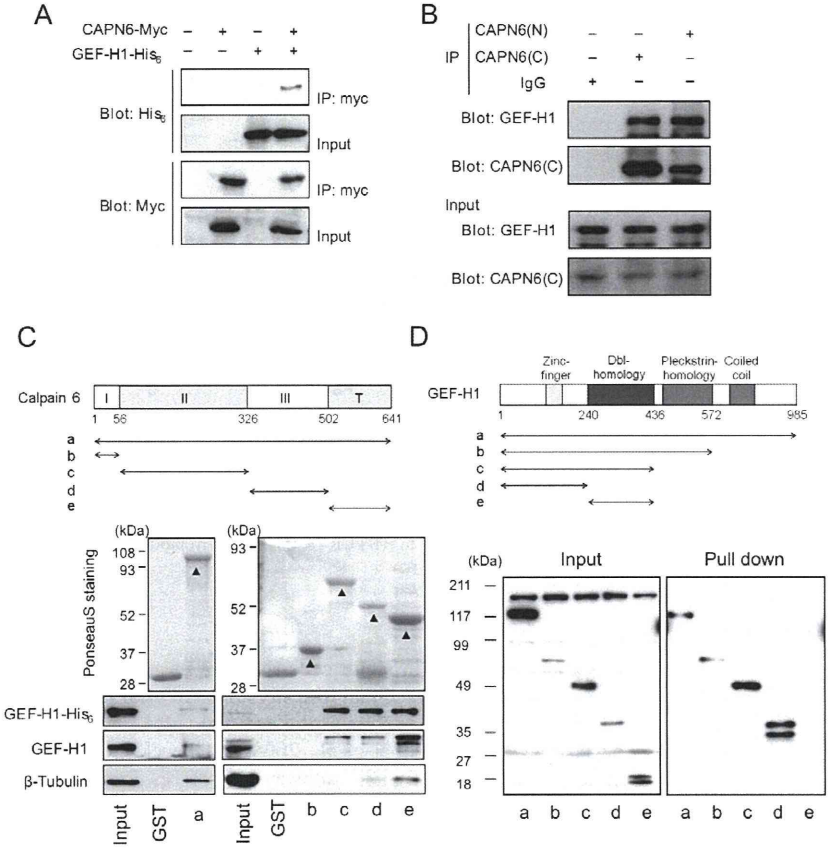

Fig. 6. Interaction of CAPN6 with GEF-H1. (**A**) GEF-H1–His_6 is coimmunoprecipitated with CAPN6–Myc. Extracts from NIH 3T3 cells transfected with each indicated vector were immunoprecipitated (IP) with anti-Myc antibody prebound to agarose beads and then subjected to immunoblotting (Blot) with an anti-His_6 antibody. (**B**) Endogenous GEF-H1 and CAPN6 interact with each other. Extracts from untransfected NIH 3T3 cells were immunoprecipitated with two different antibodies, against the CAPN6 N- [CAPN6(N)] and C-termini [CAPN6(C)], and were then immunoblotted with an anti-GEF-H1 antibody. (**C**) GST pull-down assay for the CAPN6–GEF-H1 interaction and domain mapping with GST-fused CAPN6 derivatives. GEF-H1–His_6 and GEF-H1 were pulled down from GEF-H1–His_6-expressing NIH 3T3 cell lysates containing GST-fused full-length CAPN6 (a), CAPN6 domain II (amino acids 57–326; c), CAPN6 domain III (amino acids 327–503; d) and CAPN6 domain T (amino acids 504–641; e), but not by GST-fused CAPN6 domain I (amino acids 1–56; b) or GST alone. The amounts of GST fusion proteins were grossly estimated by Ponceau staining. Arrowheads indicate GST fusion proteins. (**D**) GST pull-down assay for mapping of the GEF-H1 domains interacting with CAPN6 domain II. His_6-tagged full-length GEF-H1 (a) and its deletion mutants (b–e) were in vitro translated and subjected to the pull-down assay. His_6-tagged full-length GEF-H1 and its derivatives containing the N-terminal region (amino acids 1–240) were pulled down by GST-fused CAPN6 domain II.

and mice, whereas this residue is conserved in all other mammalian calpain members (Dear et al., 1997). Indeed, the present study and our previous results (Tonami et al., 2007) demonstrate that the effects of *Capn6* knockdown and overexpression are not affected by calpain inhibitors, indicating that the microtubule association and/or stabilization, and the GEF-H1-mediated Rac1 activation seen upon *Capn6* knockdown, are independent of the proteolytic activity. Recently, non-proteolytic functions of other mammalian calpains have been suggested following gene-targeting studies in mice (Hata et al., 2010; Ojima et al., 2010). Although calpains have proteolytic activities, they might also function as structural regulators and chaperones for other molecules. These findings might shed light on the concealed side of non-proteolytic calpain functions.

Biochemical analysis and immunostaining indicated that there was a direct interaction between CAPN6 and GEF-H1. The GST pull-down assay suggests that it was domain II of CAPN6, a cysteine protease domain in other calpain members, and the zinc-finger-containing N-terminal region of GEF-H1, that are most likely to mediate this interaction. We have previously reported that CAPN6 stabilizes microtubules through interactions mediated by domain III and, to a lesser extent, domain T (Tonami et al., 2007). However, the microtubule binding of GEF-H1 involves the N-terminal region, as well as the C-terminal and Dbl-homology domains (Krendel et al., 2002; Zenke et al., 2004). Mutations in the N-terminal region of GEF-H1 abolish its binding to microtubules and, thereby, increase its enzymatic activity (Krendel et al., 2002; Zenke et al., 2004). Thus, CAPN6 might reinforce the association between GEF-H1 and microtubules, and negatively regulate GEF-H1 activity by interacting with this region, although it remains to be resolved whether microtubule binding is necessary for the inhibition of GEF-H1 by CAPN6. The zinc-finger-containing N-terminal region of GEF-H1 contains a domain similar to the C1 diacylglycerol-binding domain of the atypical protein kinase C (aPKC) family (Birkenfeld et al., 2008). Interestingly, CAPN6 domains III and T have a similarity to the C2 domain, a Ca^{2+}- and phospholipid-binding module (Croall and Ersfeld, 2007; Goll et al., 2003). The C1 and C2 domains are known to interact within several PKC isozymes in order to determine selective lipid binding and membrane interactions (Colon-Gonzalez and Kazanietz, 2006). Thus, the interaction between CAPN6 and GEF-H1 might involve the C1 and C2 domains from each other assembling to create a functional unit.

The absence of CAPN6 is likely to cause increased microtubule instability and release of GEF-H1. Previous studies have shown that GEF-H1 is released and activated upon microtubule depolymerization (Birukova et al., 2006; Chang et al., 2008; Krendel et al., 2002). Therefore, a destabilization of microtubules caused by inactivation of CAPN6 might be responsible for GEF-H1-dependent Rac1 activation. Furthermore, the microtubule co-sedimendation assay in the presence of paclitaxel demonstrated that the affinity of GEF-H1 for stabilized microbtubules was decreased upon knockdown of *Capn6*, suggesting that CAPN6 potentiates the GEF-H1–microtubule association. However, nocodazole-induced microtubule destabilization did not recapitulate the effect of CAPN6 knockdown on Rac1 activation and

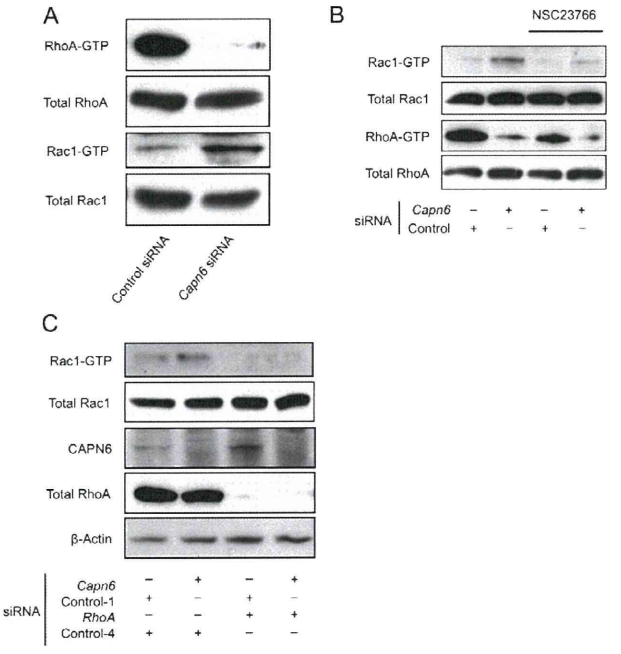

Fig. 7. Crosstalk among CAPN6, RhoA and Rac1. (**A**) Active Rho assay. The amounts RhoA-GTP were decreased in *Capn6*-siRNA-transfected cells compared with those in control-siRNA-transfected cells. (**B**) Addition of Rac1 inhibitor (50 μM NSC23766 for 16 hours) did not affect the decrease in the amounts of RhoA-GTP in *Capn6*-siRNA-transfected cells. (**C**) The activation of Rac1 induced by *Capn6* siRNA was abolished by co-transfection of *RhoA* siRNA. Data were confirmed by two independent experiments.

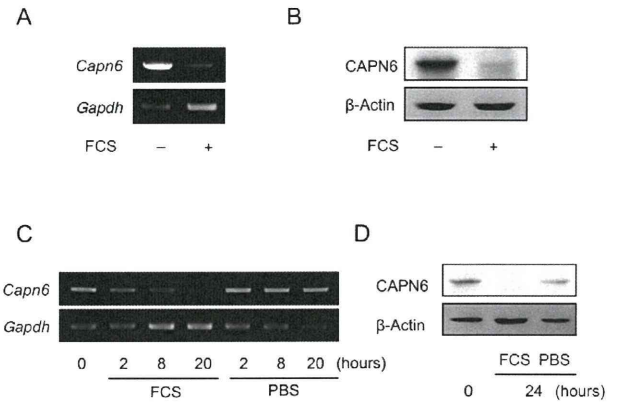

Fig. 8. Serum suppresses the expression of CAPN6 in NIH 3T3 cells. (**A**,**B**) NIH 3T3 cells were cultured in DMEM in the presence (+) or absence (–) of 10% FCS for 24 hours. (**C**,**D**) NIH 3T3 cells were stimulated with 10% FCS for the indicated times after a 12-hour starvation. Total RNA samples and cell lysates were subjected to RT-PCR (A,C) or western blotting (B,D), respectively.

lamellipodial formation (K.T., unpublished data). Thus, destabilization of microtubules is insufficient for GEF-H1-dependent Rac1 activation and lamellipodial formation. Inactivation or disappearance of CAPN6 and/or subsequent cytoskeletal changes, such as enhanced microtubule turnover, are required for translocation of GEF-H1 to the leading edge and Rac1 activation. CAPN6 might prevent GEF-H1 from translocating to the lamellipodia, to activate Rac1, even in a microtubule-free state. We present a model of CAPN6-regulated microtubule–actin crosstalk mediated by GEF-H1 in Fig. 9.

Although GEF-H1 released from microtubules has been shown to activate RhoA in some studies (Birukova et al., 2006; Chang et al., 2008; Krendel et al., 2002), RhoA activity was downregulated in cells upon *Capn6* knockdown. In this situation, GEF-H1 released from microtubules might fail to access and/or activate RhoA and would then interact with Rac1 and activate it. Although the mechanism of *Capn6*-knockdown-induced RhoA inactivation remains unknown, it might explain why GEF-H1 activates Rac1 instead of RhoA upon *Capn6* knockdown.

At the moment, it remains unclear whether the Rac1 activation by GEF-H1 is a direct effect or whether it is mediated by RhoA. Contrary to the downregulation of RhoA activity, Rac1 activation in cells upon *Capn6* knockdown was abolished by *RhoA* knockdown, indicating that this Rac1 activation appears to be dependent on RhoA. Recently, Nalbant and colleagues have reported that siRNA-induced GEF-H1 depletion causes localized RhoA inactivation at the leading edge, resulting in decreased directional migration in HeLa cells (Nalbant et al., 2009). Other reports have demonstrated that RhoA is activated prior to Rac1 and Cdc42, and functions upstream of Rac1 and Cdc42 activation at the leading edge (El-Sibai et al., 2008; Machacek et al., 2009). Although the RhoA–ROCK pathway suppresses Rac1 activity, RhoA can activate Rac1 through mammalian diaphanous homolog 1 (DIA1, also known as DIAP1), a formin family member that catalyzes actin nucleation and polymerization (Watanabe et al., 1997), when the level of RhoA activity is low (Narumiya et al., 2009; Tsuji et al., 2002). Indeed, DIA1, but not ROCK, is associated with membrane ruffles in nascent lamellipodia (Kurokawa and Matsuda, 2005) and it stabilizes microtubules specifically in leading

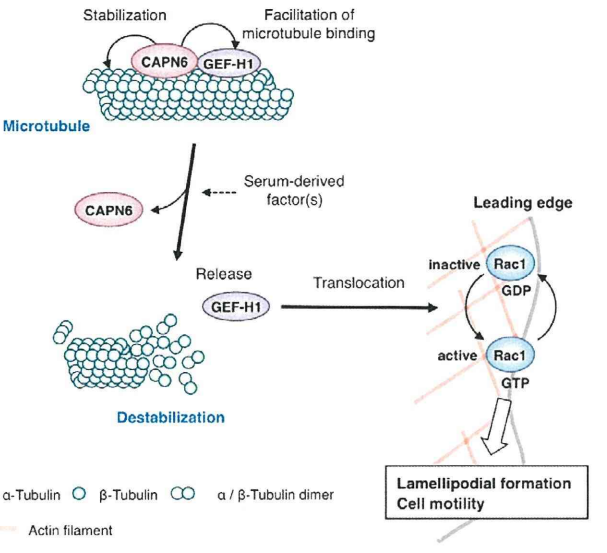

Fig. 9. Proposed model for the involvement of CAPN6–GEF-H1 interaction in Rac1-mediated lamellipodial formation and enhanced cell motility. For details, see the Discussion.

edge adhesions (Palazzo et al., 2001). Together with these findings, our present data suggest that, in the absence of CAPN6, GEF-H1 could activate Rac1, possibly through a RhoA-DIA1-dependent mechanism at the leading edge, in a spatiotemporally controlled manner in certain types of cells. Further experiments are required to determine how RhoA activity is suppressed upon CAPN6 inactivation, whether GEF-H1 can directly catalyze nucleotide exchange on Rac1 and how GEF-H1-induced RhoA and Rac1 activation is interrelated.

Here, we propose a function for non-proteolytic calpains in microtubule–actin crosstalk which is mediated through Rho family GTPase regulation. CAPN6 shares common structural characteristics with other calpain family members, such as Capn5 and *C. elegans* TRA-3 (Barnes and Hodgkin, 1996; Dear et al., 1997; Mugita et al., 1997), constituting an evolutionarily conserved subfamily. Although CAPN5 and TRA-3 are proteolytic calpains, it might be interesting to examine whether this non-proteolytic activity is also shared by these calpains and whether it is conserved across species.

Materials and Methods

Reagents

NSC23766, Y-27632 and calpeptin were purchased from Calbiochem. ZLLal was from Peptide Institute (Osaka, Japan). PDGF-BB, paclitaxel and nocodazole were from Sigma.

Plasmids

Wild-type, green fluorescent protein (GFP)-fused and glutathione transferase (GST)-fused CAPN6 expression vectors have been previously described (Tonami et al., 2007). For the expression of His_6- or Myc-tagged proteins, the open reading frames of murine *Capn6* and *GEF-H1* were subcloned, in frame, into the pcDNA3.1/V5-His TOPO (Invitrogen) or Myc-containing pcDNA3 vector (Invitrogen). All of the constructs were verified by sequencing.

RNAi

All the stealth small interfering RNA (siRNA) duplexes were synthesized by Invitrogen. Two *Capn6* siRNAs (*Capn6*-1 and *Capn6*-2) were designed to target nucleotides 1518–1542 and 1935–1959 of the mouse *Capn6* mRNA sequence (GenBank accession no. NM_007603), respectively. *Rac1* siRNA, targeting nucleotides 631–655 (GenBank accession no. NM_009007), and *RhoA* siRNA, targeting nucleotides 574–598 (GenBank accession no. NM_016802), were obtained from Invitrogen Stealth Select RNAi. For *GEF-H1* knockdown, two siRNAs (*Gef-h1*-1 and *Gef-h1*-2) were designed to target nucleotides 1085–1109 and 3410–3434 of the mouse *GEF-H1* mRNA sequence (GenBank accession no. NM_008487), respectively. As a negative control, siRNA with a scrambled sequence was prepared for each specific siRNA (Control-1 to Control-4). The sequences of siRNAs are shown in supplementary material Table S1.

Cell culture and transfection

NIH 3T3 cells were cultured in Dulbecco's modified Eagle's medium (DMEM) containing 10% fetal calf serum (FCS) and antibiotics at 37°C under 5% CO_2. For transfection, cells were grown to 50–90% confluence and were treated with a mixture of plasmid DNA and Lipofectamine LTX (Invitrogen). The siRNAs were transfected into NIH 3T3 cells using Lipofectamine RNAiMAX (Invitrogen) according to the manufacturer's protocol. After 4 hours of incubation, the cells were re-fed with medium containing FCS and were allowed to recover for 18–48 hours.

Cell migration assays

Cell migration was evaluated by the use of three methods: a three-dimensional Boyden chamber assay, a two-dimensional scratch-wound-healing assay and a random migration assay. For the Boyden chamber assay, trypsinized cells were suspended in DMEM plus 0.1% BSA and were then added to the top chambers to give a final concentration of 1.5×10^5 cells per well. The bottom chambers were filled with DMEM plus 0.1% BSA containing 100 ng/ml PDGF-BB. The polycarbonate membrane filters (8-μm-pore size) (Transwell Permeable Supports) were precoated with 5 μg of type IV collagen per filter. The migration was evaluated after a 4-hour incubation at 37°C. For the scratch wound assay, cells transfected with siRNA were starved in DMEM plus 0.5% FCS for 24 hours before the assay. The confluent cell monolayer was wounded with a plastic cell scraper. The remaining cells were washed twice with culture medium to remove cell debris and incubated at 37°C. Cell migration was evaluated at the wounded front at 6 hours after scratching. For the random migration assay, cells transfected with siRNA were cultured in DMEM plus 1% FCS for 16 hours before the assay. The cells were tracked for 4 hours at 5-minute intervals on an Olympus LCV100 microscope and were analyzed with MetaMorph software (Universal Imaging, Molecular Devices).

Cell spreading assay

At 48 hours after siRNA transfection, cells were incubated in trypsin-EDTA, until rounding but not detachment was observed, then the trypsin was carefully aspirated and fresh medium with 10% serum was added to stop the reaction. Cells were visualized by phase-contrast microscopy and scored for the percentage of spread cells at the indicated times.

Immunofluorescence microscopy

Cells were washed with preincubated general tubulin buffer (GTB) {80 mM PIPES [piperazine-N, N′-bis (2-ethanesulfonic acid)] pH 7, 1 mM $MgCl_2$ and 1 mM EGTA} at 37°C and fixed with either an ice-cold methanol and acetone mixture (1:1; for 10 minutes) or 4% paraformaldehyde in GTB for 15 minutes at room temperature. Paraformaldehyde-fixed samples were permeabilized with 0.2% Triton X-100 in GTB. Fixed cells were then washed, with GTB at room temperature, three times. After being blocked with 5% skimmed milk powder or 3% goat serum in GTB, the cells were incubated with primary antibodies against the following proteins or tags: GFP (rabbit polyclonal; MBL), His_6 (mouse monoclonal; Invitrogen), α-tubulin (mouse monoclonal, Sigma), β-tubulin (rabbit polyclonal; Sigma), GEF-H1 (mouse monoclonal; Abcam), anti-CAPN6 domain II (rabbit polyclonal Abcam) and the CAPN6 C-terminus (rabbit polyclonal; Transgenic). Then, the cells were washed, and stained with FITC- or rhodamine-conjugated donkey anti-(mouse IgG) or -(rabbit IgG) (Jackson Immunoresearch), Alexa-Fluor-488- or -555-conjugated goat anti-(mouse IgG) or -(rabbit IgG) (Molecular Probes) or DyLight-405-conjugated goat anti-(mouse IgG) (Thermo Scientific) secondary antibodies. For actin staining, 2.5 units/ml of rhodamine- or FITC-labeled phalloidin (Invitrogen) was added to the reaction buffer containing FITC-conjugated secondary antibody. The cells were viewed using a fluorescence microscope (Nikon TE300), a confocal microscope (Nikon D-ECLIPSE C1) or a LSM510 META laser-scanning confocal microscope (Carl Zeiss).

Immunoprecipitation

Cells were lysed with 0.1% NP-40 in GTB and were subjected to immunoprecipitation with the indicated antibodies using standard procedures. Myc-tagged CAPN6 was precipitated with an anti-Myc antibody (Upstate) prebound to agarose beads. For immunoprecipitation of endogenous CAPN6, the rabbit polyclonal anti-CAPN6 antibodies (N- and C-terminal specific; Transgenic) were used. Normal rabbit IgGs (Santa Cruz Biotechnology) served as negative controls.

Western blotting

For whole-cell lysate preparation, cells were solubilized in PBS containing 1% Triton X-100, 0.1% sodium deoxycholate, 0.02% SDS, 1 mM phenylmethylsulfonyl fluoride, 0.5 mM vanadate and protease inhibitor cocktail (Sigma). Cell lysates and immunoprecipitates were separated by SDS-PAGE (7.5% or 15% gels), electrotransferred onto a polyvinylidene difluoride membrane and then subjected to immunoblotting with primary antibodies against the following proteins or tags: CAPN6 (rabbit polyclonal; Transgenic), GFP (rabbit polyclonal; MBL), GEF-H1 (rabbit monoclonal; Cell Signaling Technology), GEF-H1 (mouse monoclonal; Abcam), His_6 tag (mouse monoclonal; Invitrogen), RhoA (mouse polyclonal; Santa Cruz Biotechnology), Rac1 (mouse polyclonal; Upstate), β-actin (mouse monoclonal; Sigma) and anti-tubulin or anti-(acetylated tubulin) antibodies (mouse monoclonals; Sigma). The membranes were then washed with 0.1% Tween 20 in Tris-buffered saline pH 7.6, and incubated with peroxidase-conjugated anti-(rabbit IgG) or -(mouse IgG) antibody (DAKO). The signals were detected using the enhanced chemiluminescence detection system (Amersham Bioscience) or the POD Immunostain set (Wako). The signal intensity was quantified with ImageJ 1.43 (NIH).

Rac1 and Rho activity assays

Cells were cultured in serum-free DMEM, except during experiments using Y-27632, when the DMEM was supplemented with 1% FCS. Rac1-GTP and Rho-GTP were quantified with the Rac/Cdc42 assay (PAK1-PBD, agarose conjugate) and Rho activation assay reagents (Rhotekin-RBD, agarose conjugate) (Upstate), respectively. Briefly, the cells were harvested in lysis buffer [25 mM HEPES pH 7.5, 150 mM NaCl, 1% Igepal CA-630, 10 mM $MgCl_2$, 1 mM EDTA, 10% glycerol, 1 mM phenylmethylsulfonyl fluoride, 0.5 mM vanadate and protease inhibitor cocktail (Sigma)] and then cleared lysates were incubated with the Rac/Cdc42 assay reagent or the Rho activation assay reagent for 1 hour at 4°C. Beads were washed three times with lysis buffer, and the proteins bound to the beads were separated by SDS-PAGE (15% gels) and analyzed by immunoblotting with polyclonal antibodies against Rac1 or RhoA.

GST pull-down assay

For the cell lysate preparation, NIH 3T3 cells were solubilized in pull-down buffer (20 mM Tris-HCl pH 7.6, 1% Triton-X-100, 0.25% sodium deoxycholate and 0.25 M NaCl) containing 1 mM phenylmethylsulfonyl fluoride, 0.5 mM vanadate and protease inhibitor cocktail (Sigma). Unbroken cells and cellular debris were removed by centrifugation at 20,000 ***g*** at 4°C for 15 minutes. Then, GST-fusion proteins, bound to the beads, were mixed with the lysates and incubated at 4°C for 6 hours.

The beads were washed three times with pull-down buffer containing protease inhibitors, and the bound proteins were eluted by adding 2.5× sample buffer and boiling for 5 minutes. These samples were subjected to SDS-PAGE (7.5% gels) and proteins were detected by western blotting with antibodies against His_6 or GEF-H1. The amounts of GST-fusion proteins were grossly estimated by Ponceau staining.

Microtubule co-sedimentation assay

Cells were lysed, with 1% NP-40 in GTB containing protease inhibitor cocktail (Sigma), by passing them through a 30-gauge syringe needle. After incubation on ice for 30 minutes, to depolymerize the microtubules, the lysate was centrifuged at 20,000 ***g*** for 80 minutes at 4°C to remove cellular debris. The supernatant was diluted with GTB and 0.1% NP-40, and then divided into two tubes. 20 μM Paclitaxel (Taxol) or vehicle [dimethyl sulfoxide (DMSO)] was added to each sample. After an incubation for 30 minutes at 37°C, the reaction mixture was centrifuged at 20,000 ***g*** for 40 minutes at room temperature. The resultant pellets were resuspended in lysis buffer, separated by SDS-PAGE (7.5% gels) and subjected to western blotting analysis with whole lysates or supernatants. The relative amounts of microtubule-associated GEF-H1 were estimated by the comparison of the signal intensity of GEF-H1 in pellets divided by that of total α-tubulin in whole lysates (inputs).

RT-PCR

Total RNA was extracted from NIH 3T3 cells with the use of TRIzol reagent (Invitrogen), and samples (4 μg) were then reverse-transcribed with the use of the first-strand cDNA synthesis kit (GE Healthcare) with oligo(dT) primers. The resultant cDNAs were amplified with Ex Taq polymerase (Takara) in a thermocycler. The primer sequences were 5′-GAATTCATGGGTCCTCCTCTGAAGCT-3′ (sense) and 5′-GAATTCGAGCTCAGTGAGATCATCGC-3′ (antisense) for the mouse *Capn6* mRNA, and 5′-GGTGTGAACCACGAGAAATAT-3′ (sense) and 5′-AGATCCA-CGACGGACACATT-3′ (antisense) for mouse *Gapdh* mRNA. Thermal cycling was performed for 18 to 23 cycles, to maintain PCR conditions within the linear range of amplification before saturation was reached. Each cycle consisted of 30 seconds of denaturation at 94°C, 30 seconds of annealing at 58°C and 2.5 minutes (for *Capn6*) or 30 seconds (for *Gapdh*) of extension at 72°C.

Statistical analysis

Data are expressed as means±s.e.m. Comparisons between two groups were performed using Student's *t*-tests, whereas multiple comparisons between more than two groups were analyzed by one-way ANOVA and post hoc tests. A Mann–Whitney *U*-test was used to analyze cell tracking in the random migration assay. Values of $P<0.05$ were considered statistically significant differences.

We are grateful to all the members of the Department of Physiological Chemistry and Metabolism, The University of Tokyo and the Calpain Project (Rinshoken, Tokyo, Japan) for valuable support and discussions. This work was supported in part by the Global COE Program (Integrative Life Science based on the Study of Biosignaling Mechanisms) of the Ministry of Education, Culture, Sports, Science and Technology (MEXT), Japan, and by grants-in-aid for scientific research from MEXT (grant no. 18076007 to H.S.), grants-in-aid for scientific research from the Japan Society for the Promotion of Science (grant nos 22790272 to K.T., 20590275 to Y.K., 20370055 to H.S. and 21390238 to H.K.) and grants-in-aid for scientific research from the Ministry of Health, Labour and Welfare of Japan (grant no. 09156294 to H.K.).

Supplementary material available online at
http://jcs.biologists.org/cgi/content/full/124/8/1214/DC1

References

Barnes, T. M. and Hodgkin, J. (1996). The tra-3 sex determination gene of Caenorhabditis elegans encodes a member of the calpain regulatory protease family. *EMBO J.* **15**, 4477-4484.

Benais-Pont, G., Punn, A., Flores-Maldonado, C., Eckert, J., Raposo, G., Fleming, T. P., Cereijido, M., Balda, M. S. and Matter, K. (2003). Identification of a tight junction-associated guanine nucleotide exchange factor that activates Rho and regulates paracellular permeability. *J. Cell Biol.* **160**, 729-740.

Birkenfeld, J., Nalbant, P., Yoon, S. H. and Bokoch, G. M. (2008). Cellular functions of GEF-H1, a microtubule-regulated Rho-GEF: is altered GEF-H1 activity a crucial determinant of disease pathogenesis? *Trends Cell Biol.* **18**, 210-219.

Birukova, A. A., Adyshev, D., Gorshkov, B., Bokoch, G. M., Birukov, K. G. and Verin, A. D. (2006). GEF-H1 is involved in agonist-induced human pulmonary endothelial barrier dysfunction. *Am. J. Physiol. Lung Cell. Mol. Physiol.* **290**, L540-L548.

Callow, M. G., Zozulya, S., Gishizky, M. L., Jallal, B. and Smeal, T. (2005). PAK4 mediates morphological changes through the regulation of GEF-H1. *J. Cell Sci.* **118**, 1861-1872.

Chang, Y. C., Nalbant, P., Birkenfeld, J., Chang, Z. F. and Bokoch, G. M. (2008). GEF-H1 couples nocodazole-induced microtubule disassembly to cell contractility via RhoA. *Mol. Biol. Cell* **19**, 2147-2153.

Chhabra, E. S. and Higgs, H. N. (2007). The many faces of actin: matching assembly factors with cellular structures. *Nat. Cell Biol.* **9**, 1110-1121.

Colon-Gonzalez, F. and Kazanietz, M. G. (2006). C1 domains exposed: from diacylglycerol binding to protein-protein interactions. *Biochim. Biophys. Acta* **1761**, 827-837.

Croall, D. E. and Ersfeld, K. (2007). The calpains: modular designs and functional diversity. *Genome Biol.* **8**, 218.

Dear, N., Matena, K., Vingron, M. and Boehm, T. (1997). A new subfamily of vertebrate calpains lacking a calmodulin-like domain: implications for calpain regulation and evolution. *Genomics* **45**, 175-184.

El-Sibai, M., Pertz, O., Pang, H., Yip, S. C., Lorenz, M., Symons, M., Condeelis, J. S., Hahn, K. M. and Backer, J. M. (2008). RhoA/ROCK-mediated switching between Cdc42- and Rac1-dependent protrusion in MTLn3 carcinoma cells. *Exp. Cell Res.* **314**, 1540-1552.

Enomoto, T. (1996). Microtubule disruption induces the formation of actin stress fibers and focal adhesions in cultured cells: possible involvement of the rho signal cascade. *Cell Struct. Funct.* **21**, 317-326.

Glaven, J. A., Whitehead, I., Bagrodia, S., Kay, R. and Cerione, R. A. (1999). The Dbl-related protein, Lfc, localizes to microtubules and mediates the activation of Rac signaling pathways in cells. *J. Biol. Chem.* **274**, 2279-2285.

Goll, D. E., Thompson, V. F., Li, H., Wei, W. and Cong, J. (2003). The calpain system. *Physiol. Rev.* **83**, 731-801.

Hanna, R. A., Campbell, R. L. and Davies, P. L. (2008). Calcium-bound structure of calpain and its mechanism of inhibition by calpastatin. *Nature* **456**, 409-412.

Hata, S., Abe, M., Suzuki, H., Kitamura, F., Toyama-Sorimachi, N., Abe, K., Sakimura, K. and Sorimachi, H. (2010). Calpain 8/nCL-2 and Calpain 9/nCL-4 constitute an active protease complex, G-Calpain, involved in gastric mucosal defense. *PLoS Genet.* **6**, e1001040.

Huveneers, S. and Danen, E. H. (2009). Adhesion signaling-crosstalk between integrins, Src and Rho. *J. Cell Sci.* **122**, 1059-1069.

Krendel, M., Zenke, F. T. and Bokoch, G. M. (2002). Nucleotide exchange factor GEF-H1 mediates cross-talk between microtubules and the actin cytoskeleton. *Nat. Cell Biol.* **4**, 294-301.

Kurokawa, K. and Matsuda, M. (2005). Localized RhoA activation as a requirement for the induction of membrane ruffling. *Mol. Biol. Cell* **16**, 4294-4303.

Li, R. and Gundersen, G. G. (2008). Beyond polymer polarity: how the cytoskeleton builds a polarized cell. *Nat. Rev. Mol. Cell Biol.* **9**, 860-873.

Machacek, M., Hodgson, L., Welch, C., Elliott, H., Pertz, O., Nalbant, P., Abell, A., Johnson, G. L., Hahn, K. M. and Danuser, G. (2009). Coordination of Rho GTPase activities during cell protrusion. *Nature* **461**, 99-103.

Mugita, N., Kimura, Y., Ogawa, M., Saya, H. and Nakao, M. (1997). Identification of a novel, tissue-specific calpain htra-3; a human homologue of the Caenorhabditis elegans sex determination gene. *Biochem. Biophys. Res. Commun.* **239**, 845-850.

Nalbant, P., Chang, Y. C., Birkenfeld, J., Chang, Z. F. and Bokoch, G. M. (2009). Guanine nucleotide exchange factor-H1 regulates cell migration via localized activation of RhoA at the leading edge. *Mol. Biol. Cell* **20**, 4070-4082.

Narumiya, S., Tanji, M. and Ishizaki, T. (2009). Rho signaling, ROCK and mDia1, in transformation, metastasis and invasion. *Cancer Metastasis Rev.* **28**, 65-76.

Ojima, K., Kawabata, Y., Nakao, H., Nakao, K., Doi, N., Kitamura, F., Ono, Y., Hata, S., Suzuki, H., Kawahara, H. et al. (2010). Dynamic distribution of muscle-specific calpain in mice has a key role in physical-stress adaptation and is impaired in muscular dystrophy. *J. Clin. Invest.* **120**, 2672-2683.

Palazzo, A. F., Cook, T. A., Alberts, A. S. and Gundersen, G. G. (2001). mDia mediates Rho-regulated formation and orientation of stable microtubules. *Nat. Cell Biol.* **3**, 723-729.

Ren, X. D., Kiosses, W. B. and Schwartz, M. A. (1999). Regulation of the small GTP-binding protein Rho by cell adhesion and the cytoskeleton. *EMBO J.* **18**, 578-585.

Ren, Y., Li, R., Zheng, Y. and Busch, H. (1998). Cloning and characterization of GEF-H1, a microtubule-associated guanine nucleotide exchange factor for Rac and Rho GTPases. *J. Biol. Chem.* **273**, 34954-34960.

Rodriguez, O. C., Schaefer, A. W., Mandato, C. A., Forscher, P., Bement, W. M. and Waterman-Storer, C. M. (2003). Conserved microtubule-actin interactions in cell movement and morphogenesis. *Nat. Cell Biol.* **5**, 599-609.

Siegrist, S. E. and Doe, C. Q. (2007). Microtubule-induced cortical cell polarity. *Genes Dev.* **21**, 483-496.

Tonami, K., Kurihara, Y., Aburatani, H., Uchijima, Y., Asano, T. and Kurihara, H. (2007). Calpain 6 is involved in microtubule stabilization and cytoskeletal organization. *Mol. Cell. Biol.* **27**, 2548-2561.

Tsuji, T., Ishizaki, T., Okamoto, M., Higashida, C., Kimura, K., Furuyashiki, T., Arakawa, Y., Birge, R. B., Nakamoto, T., Hirai, H. et al. (2002). ROCK and mDia1 antagonize in Rho-dependent Rac activation in Swiss 3T3 fibroblasts. *J. Cell Biol.* **157**, 819-830.

Watanabe, N., Madaule, P., Reid, T., Ishizaki, T., Watanabe, G., Kakizuka, A., Saito, Y., Nakao, K., Jockusch, B. M. and Narumiya, S. (1997). p140mDia, a mammalian homolog of Drosophila diaphanous, is a target protein for Rho small GTPase and is a ligand for profilin. *EMBO J.* **16**, 3044-3056.

Waterman-Storer, C. M., Worthylake, R. A., Liu, B. P., Burridge, K. and Salmon, E. D. (1999). Microtubule growth activates Rac1 to promote lamellipodial protrusion in fibroblasts. *Nat. Cell Biol.* **1**, 45-50.

Zenke, F. T., Krendel, M., DerMardirossian, C., King, C. C., Bohl, B. P. and Bokoch, G. M. (2004). p21-activated kinase 1 phosphorylates and regulates 14-3-3 binding to GEF-H1, a microtubule-localized Rho exchange factor. *J. Biol. Chem.* **279**, 18392-18400.

Calpain-6, a microtubule-stabilizing protein, regulates Rac1 activity and cell motility through interaction with GEF-H1

JCS072561 Supplementary Material

Files in this Data Supplement:

- **Supplemental Table S1** -

Table S1. List of siRNAs used in this study

- **Supplemental Figure S1** -

Fig. S1. Morphological changes of cells allowed to spread. NIH 3T3 cells were transfected with control- or *Capn6*-siRNA and cultured for 48 hours. Cells were then treated with trypsin-EDTA to induce rounding without detachment. Morphological changes were recorded at the indicated times after the trypsin had been aspirated and cells refed with fresh medium with 10% fetal calf serum (to stop the trypsin activity).

- **Supplemental Figure S2** -

Fig. S2. Rhodamine–phalloidin staining for actin filaments and Rac1 activity in control- and *Capn6*-siRNA-transfected cells and the effect of calpain inhibitorsA) Formation of actin-rich lamellipodia was enhanced in *Capn6*-knockdown cells. (**B**) Enhanced formation of actin-rich lamellipodia in *Capn6*-knockdown cells was not affected by the treatment with calpain inhibitors, ZLLal (100 μM) or calpeptin (50 μM). (**C**) Rac1 activity in control and *Capn6* siRNA-transfected cells in the absence or presence of ZLLal. ZLLal did not affect Rac1activity both in control and *Capn6* siRNA-transfected cells.

- **Supplemental Figure S3** -

Fig. S3. Rhodamine–phalloidin staining for actin filaments. (**A**) Control and *Capn6*-siRNA-transfected cells co-transfected with control- or *Rac1*-siRNA, or treated with Rac1 inhibitor NSC23766 (50 μM for 16 hours). (**B**) Enhanced formation of actin-rich lamellipodia in *Capn6*-knockdown cells was abrogated by *Rac1* siRNA and Rac1 inhibitor.

- **Supplemental Figure S4** -

Fig. S4. Co-immunostaining for Capn6 and tubulin in control and *Capn6* siRNA-transfected cells. Signals from two different anti-Capn6 antibodies, anti-C-terminus (**A**) and anti-Domain II (**B**), were largely overlapped with tubulin signals and diminished in *Capn6*-siRNA-transfected cells. The black-and-white pictures show rhodamine–phalloidin staining for actin.

- **Supplemental Figure S5** -

Fig. S5. Co-immunostaining for GEF-H1 and tubulin in control and *Gef-h1*-siRNA-transfected cells. Signals from the anti-GEF-H1 antibody were largely overlapped with tubulin signals and diminished in *Gef-h1*-siRNA-transfected cells (**A**). Reduction in GFF-H1 protein levels by *Gfh-h1*-siRNA was confirmed by western blotting with the same antibody (**B**).

- **Supplemental Figure S6** -

  Fig. S6. Rhodamine–phalloidin staining for actin filaments in control and *Capn6*- and/or *Gef-h1*-siRNA-transfected cells. The enhancement of lamellipodial protrusion induced by *Capn6* knockdown was suppressed by *Gef-h1*-siRNA transfection.

- **Supplemental Figure S7** -

  Fig. S7. Densitometric analysis of GEF-H1 and tubulin signals along the long axis in control and *Capn6* siRNA-transfected cells. Whereas the intensity of GEF-H1 (green) and tubulin (red) signals (the blue arrows in immunostaining pictures indicate the long axis) were well correlated to each other in the cytoplasm of control siRNA-transfected cells, the correlation was disrupted in *Capn6*-siRNA-transfected cells. The horizontal line on each graph indicates the position of nucleus.

- **Supplemental Figure S8** -

  Fig. S8. Immunostaining for GEF-H1 and Rhodamine–phalloidin staining for actin filaments. GHF-H1 signals were detected in the lamellipodial region in *Capn6*-siRNA-transfected cells. Lamellipodial translocation of GEF-H1 was not observed in PDGF-BB- or Y-27632-treated cells.

- **Supplemental Figure S9** -

  Fig. S9. Co-immunoprecipitation of endogenous Capn6 and GEF-H1 from NIH 3T3 cell lysates in the absence and presence of 5 μM nocodazole for 16 hours. GEF-H1 was co-precipitated with Capn6 similarly in both conditions.

- **Supplemental Figure S10** -

  Fig. S10. Comparison of the effects of *GEF-H1* knockdown on lamellipodial formation in *Capn6* siRNA-transfected and Y-27632-treated cells. (**A**) Rhodamine–phalloidin staining for actin filaments. (**B**) Quantitative analysis of the percentage of lamellipodia-forming cells. For each group, 100–120 cells were evaluated. *Gef-h1*-siRNA suppressed *Capn6*-siRNA-induced lamellipodial formation, but did not affect Y-27632-induced lamellipodial formation (means±s.e.m.; n=3; Fisher□s test; N.S., not significant).

- **Supplemental Figure S11** -

  Fig. S11. Rac1-GTP levels (A) and rhodamine–phalloidin staining for actin filaments (B) in control and *Capn6* siRNA-transfected cells in the absence and presence of Y-27632. ROCK inhibition with 10 μM Y-27632 for 20 minutes did not affect Rac1 activation and enhanced lamellipodial formation in *Capn6* siRNA-transfected cells.

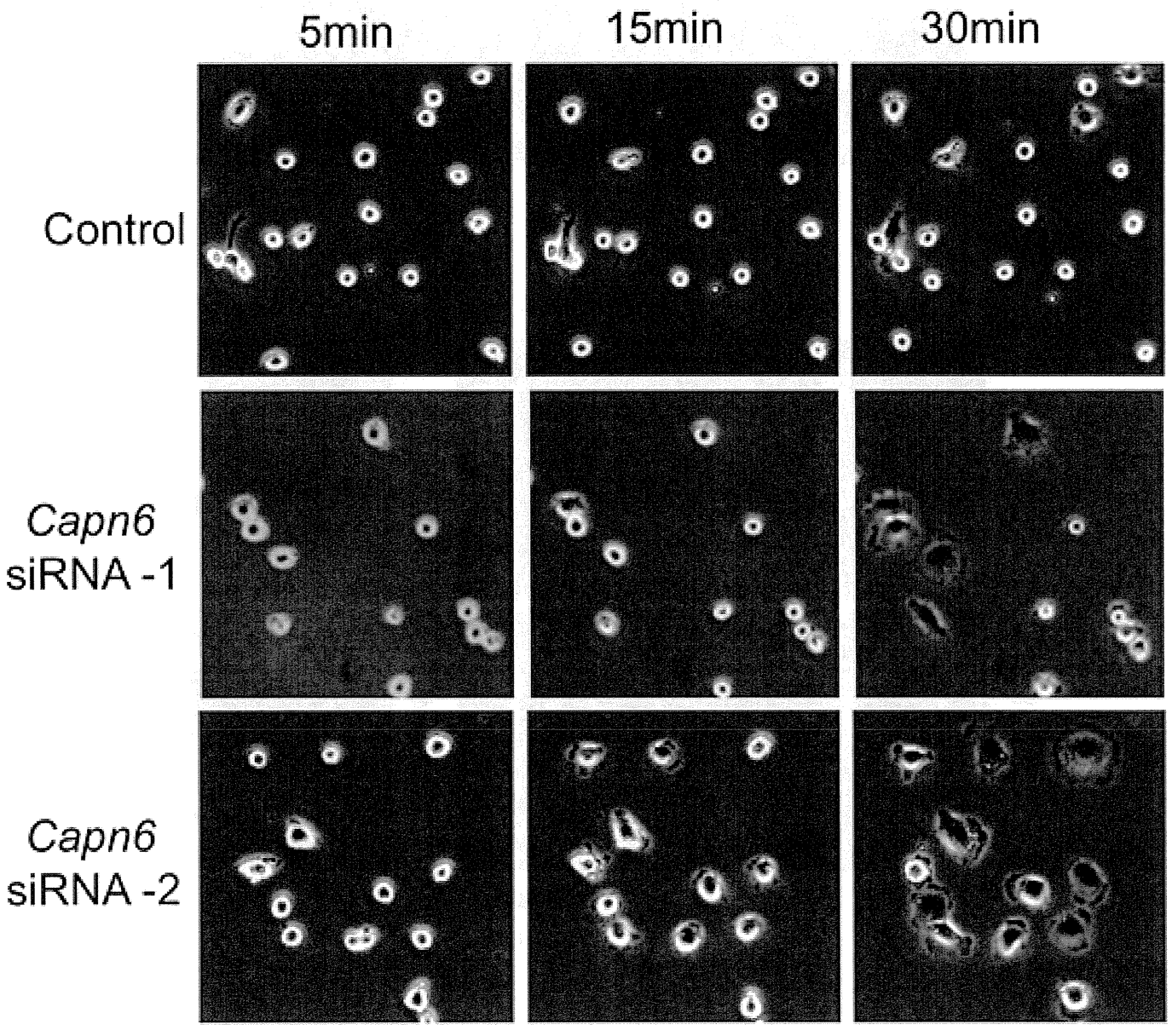
5min
15min
30min
Control
Capn6
siRNA -1
Capn6
siRNA -2